1. Extended Data

Complete the Inventory below for all Extended Data figures.

- Keep Figure Titles to one sentence only
- Upload your files as 'Figure Files' in our Manuscript Tracking system
- File names should include the Figure Number. i.e.: *Smith_ED_Fig1.jpg*
- Please be sure to include the file extension in the Filename. Note that Extended Data files must be submitted as .jpg, .tif or .eps files *only*, and should be approximately 10MB
- All Extended Data figure legends must be provided in the Inventory below and should not exceed 300 words each *(if possible)*
- Please include Extended Data *ONLY* in this table

Figure #	**Figure title** **One sentence only**	**Filename** **This should be the name the file is saved as when it is uploaded to our system. Please include the file extension. i.e.: *Smith_ED_Fig1.jpg***	**Figure Legend** **If you are citing a reference for the first time in these legends, please include all new references in the main text Methods References section, and carry on the numbering from the main References section of the paper. If your paper does not have a Methods section, include all new references at the end of the main Reference list.**
Extended Data Fig. 1	Regional association plots for rs2266590 and rs2239573 for plasma IL-10RB, *IL10RB* gene expression, and COVID-19 hospitalization.	Gaziano_ED_Fig 1.jpg	This region was investigated further using IL-10RB pQTL data because it was available on an independent proteomic platform (Olink) and results using eQTL instruments for *IL10RB* passed our Mendelian randomization *P* value threshold (0.05 Bonferroni-corrected for 1,263 actionable druggable genes) and colocalization threshold (PP.H4>0.8). **a,** rs2266590 as pQTL for plasma IL-10RB measured by Olink in 4,998 INTERVAL participants. **b,** rs2266590 as an eQTL for *IL10RB* expression tibial artery tissue (*N*=584). **c,** rs2266590 in COVID-19 hospitalization. **d,** rs2239573 as pQTL for plasma IL-10RB (after adjusting for rs2266590) measured by Olink in 4,998 INTERVAL participants. **e,** rs2239573 as an eQTL for *IL10RB* expression in whole blood (*N*=670). **f,** rs2239573 in COVID-19

			hospitalization. **a** colocalizes with **b** (PP.H4=0.97), and **d** colocalizes with **e** (PP.H4=1.00). The two variants highlighted in this figure (rs2266590 and rs2239573), which are associated with gene expression and plasma protein levels of IL-10RB, are not associated with COVID-19 hospitalization (*P*=0.85 for rs2266590, *P*=0.66 for rs2239573).
Extended Data Fig. 2	Enrichment analysis of peak eQTLs for *IFNAR2-IL10RB* and *ACE2* regions.	Gaziano_ED_Fig 2.jpg	Results obtained from association analysis using all 49 tissues from GTEx V8 contrasted against variant genotypes in an additive model. Dotplot of over-representation analysis using all significant (p<0.05) differentially expressed (DE) genes (476 for rs13050728; 1,397 for rs4830976) for **a,** rs13050728, peak eQTL in the *IFNAR2-IL10RB* region and **b,** rs4830976, peak eQTL in the *ACE2* region. Count = number of DE genes part of the enriched pathway. Gene ratio is the rate of DE genes represented in each pathway.
Extended Data Fig. 3	Regional association plots for *cis*-variants associated with *ACE2* gene expression or ACE2 plasma protein levels, and their association with COVID-19 hospitalization.	Gaziano_ED_Fig 3.jpg	**a,** rs4830976 as an eQTL for *ACE2* expression in brain frontal cortex tissue (*N*=175). **b,** rs4830976 in COVID-19 hospitalization (*N*=1,377,758). **c,** rs5935998 as the primary pQTL for plasma ACE2 measured by Oink in 4,998 INTERVAL participants **d,** rs5935998 in COVID-19 hospitalization **e,** rs4646156 as the secondary pQTL (i.e. after adjusting for rs5935998) for plasma ACE2 measured by Oink in 4,998 INTERVAL participants. **f,** rs4646156 in COVID-19 hospitalization. **a** colocalizes with **b** (PP.H4=0.95), but **c** does not colocalize with **d** (PP.H4=0.49) and **e** does not colocalize with **f** (PP.H4=0.08).

Delete rows as needed to accommodate the number of figures (10 is the maximum allowed).

2. Supplementary Information:

A. Flat Files

Complete the Inventory below for all additional textual information and any additional Supplementary Figures, which should be supplied in one combined PDF file.

- **Row 1:** A combined, flat PDF containing any Supplementary Text, Discussion, Notes, Additional Supplementary Figures, Supplementary Protocols, simple tables, and all associated legends. Only one such file is permitted.

- **Row 2:** Nature Research's Reporting Summary; if previously requested by the editor, please provide an updated Summary, fully completed, without any mark-ups or comments. **(Reporting Summaries are not required for all manuscripts.)**

Item	**Present?**	**Filename** **This should be the name the file is saved as when it is uploaded to our system, and should include the file extension. The extension must be .pdf**	**A brief, numerical description of file contents.** **i.e.:** ***Supplementary Figures 1-4, Supplementary Discussion, and Supplementary Tables 1-4.***
Supplementary Information	Yes	Supplementary_Information.pdf	Supplementary Methods and Supplementary Figures 1-2
Reporting Summary	Yes	nr-reporting-summary.pdf	

B. Additional Supplementary Files

Complete the Inventory below for all additional Supplementary Files that cannot be submitted as part of the Combined PDF.

- Do not list Supplementary Figures in this table (see section 2A)
- Where possible, include the title and description within the file itself

- Spreadsheet-based tables & data should be combined into a workbook with multiple tabs, not submitted as individual files.
- Compressed files are acceptable where necessary. ZIP files are preferred.
- Please note that the *ONLY* allowable types of additional Supplementary Files are:

  - Supplementary Tables
  - Supplementary Audio
  - Supplementary Videos
  - Supple
  - Supplementary Data, for example: raw NMR Data, Cryo-EM Data, Computational Data, Crystallo

Type	**Number** If there are multiple files of the same type this should be the numerical indicator. i.e. "1" for Video 1, "2" for Video 2, etc.	**Filename** This should be the name the file is saved as when it is uploaded to our system, and should include the file extension. i.e.: *Smith_Supplementary_Video_1.mov*	**Legend or Descriptive Caption** Describe the contents of the file
Supplementary Table	1-16	supplementary_tables.xlsx	Supplementary Tables 1–16

Editor summary: Large-scale Mendelian randomization and colocalization analyses using gene expression and soluble protein data for 1,263 actionable druggable genes, which encode protein targets for approved drugs or drugs in clinical development, identify IFNAR2 and ACE2 as the most promising therapeutic targets for early management of COVID-19.

Editor recognition statement: Joao Monteiro was the primary editor on this article and managed its editorial process and peer review in collaboration with the rest of the editorial team.

Reviewer recognition statement: Nature Medicine thanks David Evans, Steven Wolinsky, and the other, anonymous, reviewers for their contribution to the peer review of this work.

Actionable druggable genome-wide Mendelian randomization identifies repurposing opportunities for COVID-19

Liam Gaziano[1,2], Claudia Giambartolomei[3,4], Alexandre C Pereira[5,6], Anna Gaulton[7], Daniel C Posner[1], Sonja A Swanson[8], Yuk-Lam Ho[1], Sudha K Iyengar[9,10], Nicole M Kosik[1], Marijana Vujkovic[11,12], David R Gagnon[13,1], A Patrícia Bento[7], Inigo Barrio-Hernandez[14], Lars Rönnblom[15], Niklas Hagberg[15], Christian Lundtoft[15], Claudia Langenberg[16,17], Maik Pietzner[17], Dennis Valentine[18,19], Stefano Gustincich[3], Gian Gaetano Tartaglia[3], Elias Allara[2], Praveen Surendran[2,20,21,22], Stephen Burgess[23,2], Jing Hua Zhao[2], James E Peters[24,25], Bram P Prins[2,21], Emanuele Di Angelantonio[2,20,21,26,27], Poornima Devineni[1], Yunling Shi[1], Kristine E Lynch[28,29], Scott L DuVall[28,29], Helene Garcon[1], Lauren O Thomann[1], Jin J Zhou[30,31], Bryan R Gorman[1], Jennifer E Huffman[32], Christopher J O'Donnell[33,34], Philip S Tsao[35,36], Jean C Beckham[37,38], Saiju Pyarajan[1,39], Sumitra Muralidhar[40], Grant D Huang[40], Rachel Ramoni[40], Pedro Beltrao[14], John Danesh[2,20,21,26,27], Adriana M Hung[41,42], Kyong-Mi Chang[43,44], Yan V Sun[45,46], Jacob Joseph[47,1], Andrew R Leach[7], Todd L Edwards[48,49], Kelly Cho[1,50], J Michael Gaziano[1,50], Adam S Butterworth[2,20,21,26,27], Juan P Casas[1,50] on behalf VA Million Veteran Program COVID-19 Science Initiative

[1]Massachusetts Veterans Epidemiology Research and Information Center (MAVERIC), VA Boston Healthcare System, Boston, MA, USA

[2]BHF Cardiovascular Epidemiology Unit, Department of Public Health and Primary Care, University of Cambridge, Cambridge, UK

[3]Central RNA Lab, Istituto Italiano di Tecnologia, Genova, Italy

[4]Department of Pathology and Laboratory Medicine, David Geffen School of Medicine, University of California Los Angeles, Los Angeles, CA, USA

[5]Laboratory of Genetics and Molecular Cardiology, Heart Institute, University of Sao Paulo, Sao Paulo, Brazil

[6]Genetics Department, Harvard Medical School, Harvard University, Boston, MA, USA

[7]Chemical Biology, European Molecular Biology Laboratory, European Bioinformatics Institute, Hinxton, UK

[8]Department of Epidemiology, Erasmus Medical Center, Rotterdam, The Netherlands

[9]Louis Stokes Cleveland VA Medical Center, Cleveland, OH, USA

[10]Department of Population and Quantitative Health Sciences, Case Western Reserve University and Louis Stoke, Cleveland VA, Cleveland, OH, USA

[11]The Corporal Michael J. Crescenz VA Medical Center, the University of Pennsylvania Perelman School of Medicine, Philadelphia, PA, USA

[12]Medicine, Perelman School of Medicine, University of Pennsylvania, Philadelphia, PA, USA

[13]Biostatistics, School of Public Health, Boston University, Boston, MA, USA

[14]European Molecular Biology Laboratory, European Bioinformatics Institute, Hinxton, UK

[15]Department of Medical Sciences, Uppsala University, Uppsala, Sweden

[16]Berlin Insitute of Health, Charité University Medicine Berlin, Berlin, Germany

[17]MRC Epidemiology Unit, Universityof Cambridge, Cambridge, UK

[18]Institute of Health Informatics, University College London, London, UK

[19]Health Data Research, University College London, London, UK

[20]British Heart Foundation Centre of Research Excellence, University of Cambridge, Cambridge, UK
[21]Health Data Research UK Cambridge, Wellcome Genome Campus and University of Cambridge, Cambridge, UK
[22]Rutherford Fund Fellow, Department of Public Health and Primary Care, University of Cambridge, Cambridge, UK
[23]MRC Biostatistics Unit, University of Cambridge, Cambridge, UK
[24]Centre for Inflammatory Disease, Dept of Immunology and Inflammation, Imperial College, London, UK
[25]Health Data Research UK, UK
[26]National Institute for Health Research Blood and Transplant Research Unit in Donor Health and Genomics, University of Cambridge, Cambridge, UK
[27]National Institute for Health Research Cambridge Biomedical Research Centre, University of Cambridge and Cambridge University Hospitals, Cambridge, UK
[28]VA Informatics and Computing Infrastructure, VA Salt Lake City Health Care System, Salt Lake City, UT, USA
[29]Department of Internal Medicine, Epidemiology, University of Utah, Salt Lake City, UT, USA
[30]Department of Epidemiology and Biostatistics, University of Arizona, Tucson, AZ, USA
[31]Phoenix VA Health Care System, Phoenix, AZ, USA
[32]Center for Population Genomics, Massachusetts Veterans Epidemiology Research and Information Center (MAVERIC), VA Boston Healthcare System, Boston, MA, USA
[33]Cardiology, VA Boston Healthcare System, Boston, MA, USA
[34]Medicine, Brigham and Women's Hospital, Harvard Medical School, Boston, MA, USA
[35]Epidemiology Research and Information Center (ERIC), VA Palo Alto Health Care System, Palo Alto, CA, USA
[36]Department of Medicine, Stanford University School of Medicine, Palo Alto, CA, USA
[37]MIRECC, Durham VA Medical Center, Durham, NC, USA
[38]Department of Psychiatry and Behavioral Sciences, Duke University School of Medicine, Durham, NC, USA
[39]Medicine, Brigham and Women's Hospital, Harvard Medical School, Boston, MA, USA
[40]Office of Research and Development, Department of Veterans Affairs, Washington, DC, USA
[41]VA Tennessee Valley Healthcare System, Nashville, TN, USA
[42]Nephrology & Hypertension, Vanderbilt University, Nashville, TN, USA
[43]The Corporal Michael J. Crescenz VA Medical Center, Philadelphia, PA, USA
[44]Department of Medicine, Perlman School of Medicine, University of Pennsylvania, Philadelphia, PA, USA
[45]Atlanta VA Health Care System, Decatur, GA, USA
[46]Department of Epidemiology, Emory University Rollins School of Public Health, Atlanta, GA, USA

[47]Medicine, Cardiovascular, VA Boston Healthcare System and Brigham & Women's Hospital, Boston, MA, USA
[48]Department of Veterans Affairs, Tennessee Valley Healthcare System, Vanderbilt University, Nashville, TN, USA
[49]Medicine, Epidemiology, Vanderbilt Genetics Institute, Vanderbilt University Medical Center, Nashville, TN, USA
[50]Division of Aging, Brigham and Women's Hospital, Harvard Medical School, Boston, MA, USA

Authors for correspondence: asb38@medschl.cam.ac.uk (A.S.B.),

jpcasasromero@bwh.harvard.edu (J.P.C.)

Key words: Mendelian randomization, drug repurposing, COVID-19, actionable druggable genome

Abstract

Drug repurposing provides a rapid approach to meet the urgent need for therapeutics to address COVID-19. To identify therapeutic targets relevant to COVID-19, we conducted Mendelian randomization (MR) analyses, deriving genetic instruments based on transcriptomic and proteomic data for 1,263 actionable proteins that are targeted by approved drugs or in clinical phase of drug development. Using summary statistics from the Host Genetics Initiative and the Million Veteran Program, we studied 7,554 patients hospitalized with COVID-19 and >1 million controls. We found significant Mendelian randomization results for three proteins (ACE2: $P=1.6\times10^{-6}$, IFNAR2: $P=9.8\times10^{-11}$, and IL-10RB: $P=2.3\times10^{-14}$) using *cis*-eQTL genetic instruments that also had strong evidence for colocalization with COVID-19 hospitalization. To disentangle the shared eQTL signal for *IL10RB* and *IFNAR2,* we conducted phenome-wide association scans and pathway enrichment analysis, which suggested that *IFNAR2* is more likely to play a role in COVID-19 hospitalization. Our findings prioritize trials of drugs targeting IFNAR2 and ACE2 for early management of COVID-19.

INTRODUCTION

The global COVID-19 pandemic is responsible for substantial mortality, morbidity and economic hardship. Even with efficacious vaccines against the SARS-CoV-2 virus, it unknown how long it will take to achieve herd immunity, to what extent protection will diminish over time, or if future mutations will enable SARS-CoV-2 to evade immune responses stimulated by current vaccines. Hence, there is a need to rapidly identify drugs that can minimize the burden of COVID-19. Although large randomized trials have begun to successfully identity drugs that can be repurposed to address COVID-19,[1-3] most drugs evaluated so far have failed to show efficacy and have been largely confined to hospitalized or critically-ill patients. It is a priority, therefore, to identify additional drugs that can be repurposed for early management in COVID-19.

Large-scale human genetic studies are now widely used to inform drug development programs. Drug target-disease pairs supported by human genetics have a greater odds of success in drug discovery pipelines.[4] For example, identification of variants in *PCSK9* associated with lower risk of coronary disease led to the successful development of PCSK9 inhibitors, which are now licensed for prevention of cardiovascular events.[5] The value of human genetics for drug discovery and development has also been realized for infectious diseases. Human genetic studies showed that genetic variation in the *CCR5* gene provides protection against infection by human immunodeficiency virus (HIV) type-1. These findings were key for the development of Maraviroc, an antagonist of CCR5, approved by the FDA for the treatment of patients with HIV-1.[6]

Genetic variants acting in "*cis*" on druggable protein levels or gene expression that encode druggable proteins can provide powerful tools for informing therapeutic targeting, as they mimic the on-target (beneficial or harmful) effects observed by pharmacological modification.[7] Such Mendelian randomization (MR) analyses have been used to suggest repurposing opportunities for licensed drugs.[8] MR analysis that focuses on actionable druggable genes, defined as genes that encode the protein targets of drugs that are licensed or in the clinical phase of drug development, could therefore serve as a swift and robust strategy to identify drug-repurposing opportunities to prevent the complications and mortality due to COVID-19.

To identify further potential repurposing opportunities to inform trials of COVID-19 patients, we conducted large-scale MR and colocalization analyses using gene expression and soluble protein data for 1,263 actionable druggable genes that encode protein targets for approved drugs or drugs in clinical development. By combining trans-ancestry genetic data from 7,554 hospitalized COVID-19 patients and more than 1 million population-based controls from the COVID-19 Host Genetics Initiative[9] (HGI) and the Million Veteran Program[10] (MVP), we provide support for two therapeutic strategies.

RESULTS

Overall analysis plan

Figure 1 describes the overall scheme of the analyses. First, we identified all proteins that are therapeutic targets of approved or clinical-stage drugs. Next, we selected conditionally-independent genetic variants that act locally on plasma levels of these proteins or tissue-specific gene expression that encode these proteins. We proposed that these variants were instrumental variables and conduct two-sample MR analyses using a trans-ancestry meta-analysis of 7,554 cases from MVP and publicly available data (HGI outcome B2 from release 4 version 1, downloaded October 4th 2020, **Supplementary Table 1**). Given that all MR analyses relies on several assumptions, some[11] unverifiable, we conducted a multi-stage strategy to minimize confounding and biases. For MR results that passed our significance threshold after accounting for multiple testing, we performed colocalization to ensure MR results were not due to confounding by linkage disequilibrium (LD). Those with evidence of colocalization were investigated further using an independent proteomics platform (Olink). Finally, we conducted phenome-wide scans and pathway enrichment of relevant variants to reduce risks of horizontal pleiotropy and other biases due to MR violations as well as to understand potential biological mechanisms.

Actionable druggable proteins

Using data available in ChEMBL version 26, we identified 1,263 human proteins as "actionable" (i.e. therapeutic targets of approved or clinical-stage drugs) (**Supplementary Table 2**). Of these, we noted 700 proteins that are targets for drugs with potential relevance to COVID-19 from cell-based screening, registers of clinical trials against COVID-19 or approved immunomodulatory/anticoagulant drugs (given the clear role of these pathways in COVID-19

234 outcomes), or have biological evidence for the role of the protein in SARS-CoV-2 infection
235 (**Supplementary Table 3**).
236
237 **Genetic proposed instruments for actionable druggable proteins**
238 Using GTEx version 8 (V8)[12], we identified all conditionally-independent expression
239 quantitative trait loci (eQTLs) in 49 tissues that act in *cis* (within 1 Mb on either side of the
240 encoded gene), that covered 1,016 of the 1,263 druggable genes in at least one tissue
241 (**Supplementary Table 2 and 4**). We also selected *cis*-pQTLs for plasma proteins measured
242 using the SomaScan platform in 3,301 participants of the INTERVAL study[13] (**Supplementary**
243 **Table 5**) and 10,708 Fenland cohort participants[14] (**Supplementary Table 6**) that covered a total
244 of 67 proteins. In total 1,021 proteins had genetic proposed instruments using either eQTLs or
245 pQTLs, and 62 had proposed instruments using both.
246
247 **Mendelian randomization and colocalization**
248 Using our (eQTL and pQTL) proposed instruments, we performed two-sample MR on trans-
249 ancestry summary statistics for hospitalized COVID-19 cases from MVP and HGI
250 (**Supplementary Table 1)**. Using GTEx *cis*-eQTLs as proposed instruments, we found
251 significant ($P<3.96\times10^{-5}$, 0.05 Bonferroni-corrected for 1,263 actionable proteins) MR results for
252 six genes (*IL10RB*, *CCR1, IFNAR2, PDE4A, ACE2* and *CCR5)* in at least one tissue (MR results
253 with $P<3.96\times10^{-5}$ shown in **Table 1** and full MR results in **Supplementary Table 7**)**,** and four
254 additional genes (*CA5B, CA9, NSTN* and *SLC9A3*) with suggestive MR results ($P<5.00\times10^{-4}$ and
255 $P>3.96\times10^{-5}$, **Figure 2, Supplementary Table 7)**. No proposed instruments involving *cis*-
256 pQTLs reached our suggestive threshold in any of the analyses (**Supplementary Tables 8-9)**.

For three significant genes (*IL10RB, IFNAR2, ACE2*) there was strong evidence of colocalization (posterior probability of shared causal variant across two traits - hypothesis 4 [PP.H4] >0.80) between at least one proposed instrumental variant and our trans-ancestry meta-analysis of COVID-19 hospitalization (**Table 1**). Beta-coefficients of MR estimates for *ACE2* were positive in all tissues (**Table 1**), meaning higher *ACE2* expression is associated with higher risk of COVID-19 hospitalization. MR beta-coefficients for *IFNAR2* and *IL10RB* were negative and positive, respectively, in all tissues except one for each gene (skeletal muscle for *IFNAR2*; cultured fibroblasts for *IL10RB*; **Table 1**).

IL10RB and IFNAR2

Interferon alpha receptor 2 (IFNAR2) and interleukin 10 receptor beta (IL-10RB) both act as receptors for interferons (IFN). IFNAR2 forms a complex with IFNAR1, which together act as a receptor for type I IFN (IFN-α, β, ω, κ, ε), while IL-10RB acts as a receptor for type III IFN (IFN-λ) when complexed with interferon lambda receptor-1 (IFNLR1)[15], or IL-10 when complexed with IL-10RA. IL-10RB and IFNAR2 are encoded by adjacent genes and some *cis*-eQTLs for *IL10RB* are also *cis*-eQTLs for *IFNAR2* (**Supplementary Table 10, Figure 3**), making it difficult to determine which gene may be responsible for the association with COVID-19 and requiring further investigation.

All significant MR results for *IFNAR2*/*IL10RB* that colocalized with COVID-19 hospitalization contained one of nine strongly correlated (r^2>0.75 in 1000G European ancestry participants) variants (rs11911133, rs1051393, rs2300370, rs56079299, rs17860115, rs13050728, rs2236758, rs12053666, and rs1131668), which are *cis*-eQTLs for *IL10RB* in eleven tissues and for *IFNAR2* in four tissues (**Supplementary Table 11**). Within this LD block (hereafter rs13050728-LD

block), rs13050728 is the eQTL most strongly associated with COVID-19 hospitalization **(**per T-allele odds ratio = 1.17; 95% CI = 1.12-1.23; P=1.88×10^{-12}; **Supplementary Table 10**). Variants outside the rs13050728-LD block were not strongly associated with COVID-19 hospitalization (**Figure 3**).

pQTLs for IL10RB

Using stepwise conditional analysis on Olink measurements of plasma IL-10RB we identified two *cis*-pQTLs, rs2266590 (P=1.04×10^{-136}) and rs2239573 (P= 2.66×10^{-19}), which explained 5.4% and 1.2%, respectively, of the variance in plasma IL-10RB. rs2266590 was also an eQTL for *IL10RB* in three tissues and *IFNAR2* in one tissue, while rs2239573 was also an eQTL for *IL10RB* in two tissues (**Supplementary Table 11**). rs2266590 and rs2239573 lie in intron 5 and 1, respectively, of the *IL10RB* gene and are located in separate regions of high epigenetic modification (h3k27ac marking), indicating enhancer regions (**Figure 3**). rs2266590 and rs2239573 were not associated with COVID-19 hospitalization (P= 0.85 for rs2266590, P=0.66 for rs2239573, **Extended Data Fig. 1**) and MR using these two *cis*-pQTLs yields a null result (P=0.74).

A third *cis*-pQTL (rs2834167, P=1.1×10^{-8}) for plasma IL-10RB measured on the SomaScan platform was previously identified in 3,200 Icelanders over the age of 65.[16] rs2834167 is a missense variant (Lys>Glu) and is not correlated with either of the *cis*-pQTLs for plasma IL-10RB measured by Olink (r^2=0.01 for rs2266590, r^2=0.03 for rs2239573 in 1000G EUR). Although rs2834167 was associated with *IL10RB* expression in 18 tissues, it was not associated with *IFNAR2* expression in any tissue (**Supplementary Table 11**). The A allele at rs2834167,

304 which is associated with lower *IL10RB* gene expression but higher plasma IL-10RB, was
305 inversely associated with COVID-19 (per-A-allele OR= 0.91; 95%CI= 0.87-0.95; $P=5.3\times10^{-5}$).
306 Because Emilsson et al.[16] did not report full summary statistics we could not perform
307 colocalization between this pQTL and COVID-19 hospitalization. However, rs2834167 as an
308 eQTL does not colocalize (PP.H4<0.8) with COVID-19 in any tissue (**Table 1**). These three *cis*-
309 pQTLs, while possibly functional variants altering plasma IL-10RB levels, suggest that the
310 plasma IL-10RB levels are not likely the mediator of the association between this locus and
311 COVID-19 hospitalization. IFNAR2 was not measured on the SomaScan or Olink platforms.
312
313 *Phenome-wide scan of rs13050728*
314 To identify other phenotypes associated with rs13050728, we performed a phenome-wide scan
315 of GWAS for proteins measured by Olink and SomaLogic platforms in INTERVAL participants
316 (see methods), and publicly available data on PhenoScanner[17] and GTEx. rs13050728 was
317 associated with tryptase gamma 1 (TPSG1, $P= 1.5\times10^{-5}$) and vascular endothelial growth factor
318 2 (VEGFR2, $P= 2.6\times10^{-5}$, **Supplementary Table 12**), and both showed strong evidence of
319 colocalization with COVID-19 hospitalization (PP.H4=0.96 for VEGFR2, PP.H4=0.96 for
320 TPSG1, **Figure 4)**. The C allele at rs13050728 associated with higher *IFNAR2* expression in all
321 tissues (except skeletal muscle), lower risk of COVID-19 hospitalization, and lower levels of
322 plasma VEGFR2 and TPSG1 (**Supplementary Table 12**). This mimics agonistic effects of
323 IFNAR2 through recombinant type-I IFNs, which are known to have an anti-angiogenic effect, at
324 least in part through reduced VEGF/VEGFR2 signaling[18,19], and decrease tryptase levels in a
325 phase-2 trial using recombinant type-I IFN in patients with mastocytosis[20], a condition that
326 causes proliferation of mast cells. rs13050728 was not associated at $P<3.96\times10^{-5}$ (our Bonferroni

corrected *P* value) with any phenotype beyond plasma VEGFR2 and TPSG1 and gene expression of *IFNAR2* and *IL10RB* (**Supplementary Table 12**), indicating that this variant is unlikely to exhibit widespread horizontal pleiotropy. Also, the chances of substantial bias due to MR violations is low[21] since the variant is not strongly associated with other risk factors that could alter the likelihood of SARS-CoV-2 testing or hospitalization of COVID-19 patients.

Pathway enrichment analysis of rs13050728

Using information from all GTEx V8 tissues we identified 476 genes whose expression levels were associated with rs13050728 at a nominal significance level ($P < 0.05$). Taking into consideration an adjusted *P* value for multiple testing within the WikiPathway corpus, only two biological pathways were significantly associated among all 624 pathways present in this database: Host-pathogen interaction of human corona viruses - IFN induction (adjusted *P* value = 0.0028) and Type I IFN Induction and Signaling During SARS-CoV-2 Infection (adjusted *P* value = 0.0098). In addition, among Gene Ontology (GO) and Reactome pathways, several gene sets were also significantly enriched. Notably, among enriched pathways were those related to IFN type I or antiviral response (**Extended Data Fig. 2A**).

ACE2

Angiotensin converting enzyme 2 (ACE2) converts angiotensin II into angiotensin (1-7) as part of the RAA system, and more importantly, is the viral receptor for SARS-CoV-2. We identified seven *cis*-eQTLs in seven tissues (**Supplementary Table 13**) for *ACE2* which are strongly correlated (r^2>0.75 in 1000G EUR, **Supplementary Table 14**) with rs4830976 being the eQTL in the region most strongly associated with COVID-19 hospitalization.

pQTLs for ACE2

Stepwise conditional analysis for plasma ACE2 measured by Olink revealed one pQTL, rs5935998 (P=1.45×10^{-21}), which is in high LD with a previously reported *cis*-pQTL (rs12558179) for ACE2 (r^2=0.89 in 1000G EUR)[22], and a secondary suggestive signal (rs4646156, P= 3.20×10^{-7}). rs5935998 and rs4646156 are concordant in their effect on COVID-19 hospitalization (higher ACE2 levels corresponds to higher risk of COVID-19 hospitalization for both) resulting in a strong, positive MR association (MR beta-coefficient: 0.34; 95% CI: 0.17-0.51; P=8.1×10^{-5}). Although neither rs5935998 or rs4646156 strongly colocalized with COVID-19 hospitalization (PP.H4=0.49 for rs5935998, PP.H4=0.08 for rs4646156, **Extended Data Fig. 3**), the two pQTLs, while statistically independent, are mildly correlated (r^2=0.20 in 1000G EUR), which can make colocalization difficult to interpret.[23] One possible explanation is that these two pQTLs confer an effect on COVID-19 hospitalization that converges on the rs4830976-LD-block, as both are moderately correlated with rs4830976 (r^2=0.32 for rs5935998, r^2=0.42 for rs4646156 in 1000G EUR, **Extended Data Fig. 3**)

Phenome-wide scan of rs4830976

rs4830976 is associated (P<3.96×10^{-5}) with and colocalized (PP.H4>0.80) with expression of nearby genes *CA5B*, *CLTRN* (also known as *TMEM27*), and *VEGFD* (**Supplementary Table 15**) in at least one tissue, indicating that this variant may be instrumenting on gene expression beyond *ACE2*. However, given the biological prior that ACE2 acts as the receptor of SARS-CoV-2, *ACE2* is probably more likely than *CA5B*, *CLTRN* or *VEGFD* to be responsible for COVID-19 hospitalization. There were no other reported phenome-wide scan results at P

373 $<3.96\times10^{-5}$ for rs4830976, which is at least in part due to the lack of reported X-chromosome
374 results from a large proportion of GWAS.
375
376 *Pathway enrichment analysis of rs4830976*
377 Exploring the landscape of genes differentially expressed according to genotype in GTEx V8, we
378 observed 1397 genes differentially expressed at a nominal *P* value less than 0.05. Over-
379 representation analysis identified 238 significantly enriched biological pathways among
380 differentially expressed genes (**Extended Data Fig. 2B**). Among these, signaling by interleukins,
381 regulation of cytokine production, and antigen processing and presentation, might prove
382 biologically relevant in COVID-19 infection.
383

DISCUSSION

To identify drug-repurposing opportunities to inform trials against COVID-19, we conducted a large-scale MR analysis of protein and gene expression data. We first updated the "actionable" genome to an enlarged set of 1,263 human proteins and provided evidence for 700 of these as targets for drugs with some potential relevance to COVID-19. By investigating more than a thousand potential targets using several of the largest currently available human genetic datasets, we provide evidence for drug targets of type-I IFNs (IFNAR2) and ACE2 modulators (ACE2) as priority candidates for evaluation in randomized trials of early management in COVID-19.

Our finding that ACE2 may play an important role in COVID-19 is unsurprising given its well-known relevance to SARS-CoV-2. Since ACE2 acts as the primary receptor for SARS-CoV-2, increased expression of ACE2 has been hypothesized to lead to increased susceptibility to infection. ACE2 plays a vital role in the RAAS signaling pathway, providing negative regulation through the conversion of Angiotensin II to Angiotensin 1-7. This action has anti-inflammatory and cardioprotective effects[24] and plays a protective role in acute respiratory distress syndrome.[25] ACE2 is a single-pass membrane protein but can be cleaved from the membrane to a soluble form which retains the enzymatic function to cleave Angiotensin II. It has therefore been hypothesized that administration of human recombinant soluble ACE2 (hrsACE2) could be an effective treatment for COVID-19, through distinct mechanisms in two phases of COVID-19. First, hrsACE2 can bind the viral spike glycoprotein of SARS-CoV-2, which could prevent cellular uptake of SARS-CoV-2 by reducing binding to the membrane-bound form of ACE2 (early phase). This suggestion is supported by the finding that APN01, a hrsACE2 therapeutic, showed a strong reduction in SARS-CoV-2 viral load[26] and enhanced the benefit of remdesivir[27] in primate kidney epithelial (Vero) cells and human kidney organoids. In the later phase,

hrsACE2 could reduce sequelae of SARS-CoV-2 infection by reducing inflammation in the lungs and other infected tissues. A case report of a hospitalized COVID-19 patient supports this hypothesis by showing that 7-day administration of APN01 was associated with a reduction in SARS-CoV-2 viral load and inflammatory markers.[28] APN01 is currently being tested in a phase II trial to reduce mortality and invasive mechanical ventilation in 200 hospitalized COVID-19 patients[29]. Interestingly, a recent report showed that expression of a truncated ACE2 isoform, dACE2, which poorly binds with SARS-CoV-2 spike protein, is stimulated by type I, II and III IFNs in human ileum organoids[30].

One of the main challenges of our analysis was to determine whether IFNAR2 or IL10RB (or both) was driving the association with COVID-19 hospitalization, given that they share *cis*-eQTLs used as proposed instruments for our MR analysis. Multiple lines of evidence indicate that IFNAR2 appears to be primarily responsible for the signal observed. First, our phenome-wide scan using the lead *IFNAR2/IL10RB cis*-eQTL reproduced known effects of type-I IFNs (the therapeutic target of IFNAR2) on VEGFR2 and TPSG1.[18-20] Second, our pathway enrichment analysis using the same eQTL revealed pathways associated with type-I IFN receptor (IFNAR2) signaling. Last, three independent *cis*-pQTLs that are also *cis*-eQTLs for *IL10RB* did not show evidence of association with COVID-19, suggesting that plasma IL-10RB concentrations are less likely to be etiologically relevant to COVID-19.

Evidence of a role for type-I IFN in COVID-19 is rapidly emerging. Studies using *in vitro* (A549 pulmonary cell lines), animal (ferrets) and *ex vivo* (human lung tissue) models have all shown lower expression of genes encoding type-I IFNs after exposure to SARS-CoV-2 compared to other respiratory viruses.[31,32] This has been confirmed *in vivo* by studies showing significantly

impaired type-I IFN response – including almost no IFN-beta activity - in the peripheral blood of severe COVID-19 patients compared to mild to moderate COVID-19 patients.[33] More importantly, lower levels of IFN alpha-2 among recently hospitalized COVID-19 patients were associated with a substantial increase in the risk of progression to critical care, supporting our observation that lower genetically-predicted *IFNAR2* expression was associated with higher risk of COVID-19 hospitalization.[33] Additionally, auto-antibodies for type I IFNs were found in a much higher proportion of individuals with severe COVID-19 than those with asymptomatic or mild SARS-CoV-2 infection.[34]

Whole exome and genome sequencing studies on severe COVID-19 patients have identified rare mutations that implicate type I IFN signaling. Zhang *et al*.[35] found patients with severe COVID-19 were enriched for rare variants predicted to cause loss of protein function at 13 genes involved in type-I IFN response. A cases-series of four patients under the age of 35 with severe COVID-19 found a rare LOF mutation in *TLR7* and decreased type I IFN signaling.[36] The GenOMICC study of imputed GWAS on severe COVID-19 identified signals that lie in the *IFNAR2* gene.[37]

Several *in vitro* studies have found a reduction in SARS-CoV-2 replication in multiple cell types (including animal and human) and human organoids after pre-treatment with type-I or -III IFNs when compared with controls[38-41] (**Supplementary Table 16**). Though these *in vitro* studies are encouraging, evidence from randomized trials for type I IFNs in early COVID-19 stages is limited. Hung et al.[42] showed that randomization to a combination of IFN beta-1b, ribavirin and lopinavir-ritonavir was superior to lopinavir-ritonavir alone in shortening the duration of viral shedding, alleviating symptoms and reducing the length of the hospital stay. Importantly, these

benefits were confined to a subgroup who were hospitalized within 7 days of onset of symptoms when IFN beta-1b was administered to the intervention arm. These results, together with our genetic findings on COVID-19 hospitalization and the established role of type-I IFNs as first line of response against viral agents suggest recombinant type-I IFN as potential intervention during early stages of COVID-19. To date, there is no large randomized trial on IFN beta for early treatment of COVID-19 patients who are at high risk of hospitalization.

Trial evidence on the use of IFN-beta in late stages of COVID-19 has emerged very recently. The SOLIDARITY trial, which randomized 2,050 hospitalized COVID-19 patients to IFN beta-1a, found no effect on mortality overall (relative risk [RR]=1.16, 95% CI: 0.96-1.39), but the trial was not powered to evaluate a possible trend across subgroups of COVID-19 severity at randomization (RR=1.40, 95% CI: 0.82-2.40 for those on ventilator, RR=1.13, 95% CI: 0.86-1.50 for those not ventilated but on oxygen, and RR=0.80, 95% CI: 0.27-2.35 in those with neither).[43] The Adaptive COVID-19 Treatment Trial 3 (ACTT-3) stopped enrollment of severely ill COVID-19 patients for a trial on IFN beta-1a and remdesivir due to adverse events but continued enrolling patients with less severe disease.[44] The ACTT-2 found that baricitinib (an inhibitor of the JAK family of proteins, some of which are immediately downstream of *IFNAR2*) when administered to hospitalized COVID-19 patients was beneficial in severe cases but not in moderate disease[3]. These findings indicate no role for the use of IFN beta during late stages of COVID-19, when the cytokine storm is already established.

We are the first to implicate a causal role for ACE2 in COVID-19 manifestations using MR techniques; we have also implicated IFNAR2 in COVID-19, concordant with recent studies[37,45]. However, the current study importantly complements and extends previous efforts by employing

key approaches to protect against potential biases, strengthen causal inference, and enhance understanding of potential mechanisms. First, in contrast to Liu *et al*. and the GenOMICC study, the current study involved several measures to minimize potential biases. We used colocalization methods to minimize the chances of false positive results due to confounding by LD. We reduced the possible impact of bias due to horizontal pleiotropy by restricting our proposed instruments to variants acting in *cis* and performing phenome-wide scan to ensure instrumental variants were only associated/colocalized with gene expression of the tested gene or downstream phenotypes. When the possibility of horizontal pleiotropy was identified (e.g. *IFNAR2* and *IL10RB* sharing eQTLs), we addressed it using pQTL data and pathway enrichment analysis to disentangle mechanisms, ultimately showing *IFNAR2* is more likely the causal gene. Phenome-wide scans revealing effects on plasma proteins (VEGFR2 and TPSG1) that mimic known biology of type I IFN provides confidence that we are correctly instrumenting IFNAR2 and can identify on-target (harmful or beneficial) effects of administering type I IFN.

Second, our study had excellent statistical power, yielding highly significant MR associations for *IFNAR2* (P=9.8×10^{-11}), increasing confidence in the validity of the much weaker signals for *IFNAR2* reported in the GenOMICC study (P=0.004), particularly as the earlier report had displayed evidence of confounding by LD (P_{HEIDI}= 0.015).[37] Indeed, compared to the analysis on COVID-19 hospitalization by Liu *et al.*, our analysis contained more than double the number of cases.[45] Third, with our rigorous instrument selection process that used comprehensive datasets on gene expression and plasma protein levels, we were able to robustly evaluate over one thousand actionable drug targets, like ACE2, which was not evaluated in the previous MR

studies. Fourth, inclusion of MVP with HGI provided a more diverse population and identification of credible biological targets that were consistent across multiple ancestral groups.

Lastly, we provide an updated catalog of all actionable protein targets and drugs that are amenable to causal inference investigation through human genetics that can be applied to outcomes beyond COVID-19. For 700 proteins of the actionable genes, we also include information as to potential relevance to the treatment of COVID-19, which can help future studies to contextualize findings on COVID-19.

Our analysis also has limitations. Though we make use of instrumental variants from multiple data sources, they did not cover the entire actionable druggable genome or were derived from COVID-19 patients. Identifying the most relevant tissue or cell-type can be challenging for interpreting MR analyses of gene expression. In our case, a relevant tissue could be: one invaded by SARS-CoV-2, an organ associated with clinical complications of COVID-19, a tissue where the COVID-19-relevant protein is produced, or a tissue that would be the likely site of action for the target drug. We opted to use a data-driven strategy that incorporates all tissues available in GTEx V8. For *IFNAR2*, we recovered fibroblasts (the main cell type responsible for IFN-beta production), esophageal mucosa[46] (a tissue invaded by SARS-CoV-2), and skeletal muscle[47] (associated with the neurological manifestations of COVID-19). For *ACE2*, we recovered brain tissue, an organ known to be invaded by SARS-CoV-2 and associated with clinical manifestations.[48,49] Lastly, this work focused on cis-variants with an effect on gene expression and protein levels. We did not consider the full complexity of gene isoforms and splice SNPs, therefore missing mediation relationships that are isoform-specific. Also, we did not consider

other pathways through which variants may affect disease, such as DNA methylation, histone modification, chromatin accessibility and others.

In conclusion, our trans-ancestry MR analysis covering all actionable druggable genes identified two drug repurposing opportunities (type-I IFNs and hsrACE2) as interventions that need to be evaluated in adequately powered randomized trials to investigate their efficacy and safety for early management of COVID-19.

Acknowledgements

We are grateful to the Host Genetic Initiative for making their data publicly available (full acknowledgements can be found here: https://www.covid19hg.org/acknowledgements/). This research is based on data from the Million Veteran Program, Office of Research and Development, Veterans Health Administration, and was supported by award #MVP035. This research was also supported by additional Department of Veterans Affairs awards grant #MVP001. This publication does not represent the views of the Department of Veteran Affairs or the United States Government. Full acknowledgements for the VA Million Veteran Program COVID-19 Science Initiative can be found in the supplementary methods. C.G. has received funding from the European Union's Horizon 2020 research and innovation program under the Marie Skłodowska-Curie grant agreement No 754490 – MINDED project. A.G., P.B. and A.R.L. are funded by the Member States of the European Molecular Biology Laboratory (EMBL). I.B.-H. received funding from Open Targets (grant agreement OTAR-044). The Fenland Study (10.22025/2017.10.101.00001) is funded by the Medical Research Council (MC_UU_12015/1); we are grateful to all the volunteers and to the General Practitioners and practice staff for assistance with recruitment; we thank the Fenland Study Investigators, Fenland Study Co-ordination team and the Epidemiology Field, Data and Laboratory teams; we further acknowledge support for genomics from the Medical Research Council (MC_PC_13046); proteomic measurements were supported and governed by a collaboration agreement between the University of Cambridge and Somalogic. J.E.P. is supported by UKRI Innovation Fellowship at Health Data Research UK (MR/S004068/2). L.R., N.H. and C.L. are supported by the Swedish Research Council. E.A. was supported by the EU/EFPIA Innovative Medicines Initiative Joint Undertaking BigData@Heart grant n° 116074 and by the British Heart Foundation Programme

Grant RG/18/13/33946. We thank Dr. Angela Wood for feedback on statistical analyses used in the paper. We thank the INTERVAL Study investigators, co-ordination team and the epidemiology field, data and laboratory teams, which were supported by core funding from the UK Medical Research Council (MR/L003120/1), the British Heart Foundation (RG/13/13/30194; RG/18/13/33946), the NIHR Cambridge Biomedical Research Centre (BRC-1215-20014) [The views expressed are those of the author(s) and not necessarily those of the NIHR or the Department of Health and Social Care], and the NIHR Blood and Transplant Research Unit in Donor Health and Genomics (NIHR BTRU-2014-10024). This work was also supported by Health Data Research UK, which is funded by the UK Medical Research Council, the Engineering and Physical Sciences Research Council, the Economic and Social Research Council, the Department of Health and Social Care (England), the Chief Scientist Office of the Scottish Government Health and Social Care Directorates, the Health and Social Care Research and Development Division (Welsh Government), the Public Health Agency (Northern Ireland), the British Heart Foundation, and Wellcome. J.D. holds a British Heart Foundation Professorship and a National Institute for Health Research Senior Investigator Award.

References

1. Horby, P.*, et al.* Dexamethasone in Hospitalized Patients with Covid-19 - Preliminary Report. *N Engl J Med* (2020).
2. Beigel, J.H.*, et al.* Remdesivir for the Treatment of Covid-19 - Final Report. *N Engl J Med* (2020).
3. Kalil, A.C.*, et al.* Baricitinib plus Remdesivir for Hospitalized Adults with Covid-19. *New England Journal of Medicine* (2020).
4. Nelson, M.R.*, et al.* The support of human genetic evidence for approved drug indications. *Nat Genet* **47**, 856-860 (2015).
5. Cohen, J.C., Boerwinkle, E., Mosley, T.H., Jr. & Hobbs, H.H. Sequence variations in PCSK9, low LDL, and protection against coronary heart disease. *N Engl J Med* **354**, 1264-1272 (2006).
6. Lopalco, L. CCR5: From Natural Resistance to a New Anti-HIV Strategy. *Viruses* **2**, 574-600 (2010).
7. Finan, C.*, et al.* The druggable genome and support for target identification and validation in drug development. *Sci Transl Med* **9**(2017).
8. Swerdlow, D.I.*, et al.* The interleukin-6 receptor as a target for prevention of coronary heart disease: a mendelian randomisation analysis. *Lancet* **379**, 1214-1224 (2012).
9. The COVID-19 Host Genetics Initiative, a global initiative to elucidate the role of host genetic factors in susceptibility and severity of the SARS-CoV-2 virus pandemic. *Eur J Hum Genet* **28**, 715-718 (2020).
10. Gaziano, J.M.*, et al.* Million Veteran Program: A mega-biobank to study genetic influences on health and disease. *J Clin Epidemiol* **70**, 214-223 (2016).
11. Labrecque, J. & Swanson, S.A. Understanding the Assumptions Underlying Instrumental Variable Analyses: a Brief Review of Falsification Strategies and Related Tools. *Curr Epidemiol Rep* **5**, 214-220 (2018).
12. The Genotype-Tissue Expression (GTEx) project. *Nat Genet* **45**, 580-585 (2013).
13. Sun, B.B.*, et al.* Genomic atlas of the human plasma proteome. *Nature* **558**, 73-79 (2018).
14. Pietzner, M.*, et al.* Genetic architecture of host proteins involved in SARS-CoV-2 infection. *Nat Commun* **11**, 6397 (2020).
15. Borden, E.C.*, et al.* Interferons at age 50: past, current and future impact on biomedicine. *Nat Rev Drug Discov* **6**, 975-990 (2007).
16. Emilsson, V.*, et al.* Co-regulatory networks of human serum proteins link genetics to disease. *Science* **361**, 769-773 (2018).
17. Staley, J.R.*, et al.* PhenoScanner: a database of human genotype-phenotype associations. *Bioinformatics* **32**, 3207-3209 (2016).
18. von Marschall, Z.*, et al.* Effects of interferon alpha on vascular endothelial growth factor gene transcription and tumor angiogenesis. *J Natl Cancer Inst* **95**, 437-448 (2003).
19. Jia, H.*, et al.* Endothelial cell functions impaired by interferon in vitro: Insights into the molecular mechanism of thrombotic microangiopathy associated with interferon therapy. *Thromb Res* **163**, 105-116 (2018).
20. Casassus, P.*, et al.* Treatment of adult systemic mastocytosis with interferon-alpha: results of a multicentre phase II trial on 20 patients. *Br J Haematol* **119**, 1090-1097 (2002).
21. Swanson, S.A., Tiemeier, H., Ikram, M.A. & Hernán, M.A. Nature as a Trialist?: Deconstructing the Analogy Between Mendelian Randomization and Randomized Trials. *Epidemiology* **28**, 653-659 (2017).

22. Nelson, C.P., *et al.* Genetic Associations With Plasma Angiotensin Converting Enzyme 2 Concentration: Potential Relevance to COVID-19 Risk. *Circulation* **142**, 1117-1119 (2020).
23. Wallace, C. Eliciting priors and relaxing the single causal variant assumption in colocalisation analyses. *PLoS Genet* **16**, e1008720 (2020).
24. Hemnes, A.R., *et al.* A potential therapeutic role for angiotensin-converting enzyme 2 in human pulmonary arterial hypertension. *Eur Respir J* **51**(2018).
25. Kuba, K., Imai, Y., Rao, S., Jiang, C. & Penninger, J.M. Lessons from SARS: control of acute lung failure by the SARS receptor ACE2. *J Mol Med (Berl)* **84**, 814-820 (2006).
26. Monteil, V., *et al.* Inhibition of SARS-CoV-2 Infections in Engineered Human Tissues Using Clinical-Grade Soluble Human ACE2. *Cell* **181**, 905-913.e907 (2020).
27. Monteil, V., *et al.* Human soluble ACE2 improves the effect of remdesivir in SARS-CoV-2 infection. *EMBO Mol Med* **13**, e13426 (2020).
28. Zoufaly, A., *et al.* Human recombinant soluble ACE2 in severe COVID-19. *Lancet Respir Med* (2020).
29. Recombinant Human Angiotensin-converting Enzyme 2 (rhACE2) as a Treatment for Patients With COVID-19. (https://ClinicalTrials.gov/show/NCT04335136).
30. Onabajo, O.O., *et al.* Interferons and viruses induce a novel truncated ACE2 isoform and not the full-length SARS-CoV-2 receptor. *Nat Genet* **52**, 1283-1293 (2020).
31. Blanco-Melo, D., *et al.* Imbalanced Host Response to SARS-CoV-2 Drives Development of COVID-19. *Cell* **181**, 1036-1045.e1039 (2020).
32. Chu, H., *et al.* Comparative Replication and Immune Activation Profiles of SARS-CoV-2 and SARS-CoV in Human Lungs: An Ex Vivo Study With Implications for the Pathogenesis of COVID-19. *Clin Infect Dis* **71**, 1400-1409 (2020).
33. Hadjadj, J., *et al.* Impaired type I interferon activity and inflammatory responses in severe COVID-19 patients. *Science* **369**, 718-724 (2020).
34. Bastard, P., *et al.* Auto-antibodies against type I IFNs in patients with life-threatening COVID-19. *Science* (2020).
35. Zhang, Q., *et al.* Inborn errors of type I IFN immunity in patients with life-threatening COVID-19. *Science* (2020).
36. van der Made, C.I., *et al.* Presence of Genetic Variants Among Young Men With Severe COVID-19. *Jama* **324**, 1-11 (2020).
37. Pairo-Castineira, E., *et al.* Genetic mechanisms of critical illness in Covid-19. *Nature* (2020).
38. Lokugamage, K.G., *et al.* Type I Interferon Susceptibility Distinguishes SARS-CoV-2 from SARS-CoV. *Journal of Virology* **94**, e01410-01420 (2020).
39. Mantlo, E., Bukreyeva, N., Maruyama, J., Paessler, S. & Huang, C. Antiviral activities of type I interferons to SARS-CoV-2 infection. *Antiviral Res* **179**, 104811 (2020).
40. Clementi, N., *et al.* Interferon-β-1a Inhibition of Severe Acute Respiratory Syndrome-Coronavirus 2 In Vitro When Administered After Virus Infection. *J Infect Dis* **222**, 722-725 (2020).
41. Dinnon, K.H., *et al.* A mouse-adapted model of SARS-CoV-2 to test COVID-19 countermeasures. *Nature* **586**, 560-566 (2020).
42. Hung, I.F., *et al.* Triple combination of interferon beta-1b, lopinavir-ritonavir, and ribavirin in the treatment of patients admitted to hospital with COVID-19: an open-label, randomised, phase 2 trial. *Lancet* **395**, 1695-1704 (2020).
43. Repurposed Antiviral Drugs for Covid-19 — Interim WHO Solidarity Trial Results. *New England Journal of Medicine* (2020).
44. NIAID Stops COVID-19 Trial Enrollment Over Adverse Events. (2020).
45. Liu, D., *et al.* Mendelian randomization analysis identified genes pleiotropically associated with the risk and prognosis of COVID-19. *J Infect* (2020).

46. Xiao, F., *et al.* Evidence for Gastrointestinal Infection of SARS-CoV-2. *Gastroenterology* **158**, 1831-1833.e1833 (2020).
47. Mao, L., *et al.* Neurologic Manifestations of Hospitalized Patients With Coronavirus Disease 2019 in Wuhan, China. *JAMA Neurol* **77**, 683-690 (2020).
48. Song, E., *et al.* Neuroinvasion of SARS-CoV-2 in human and mouse brain. *J Exp Med* **218**(2021).
49. Puelles, V.G., *et al.* Multiorgan and Renal Tropism of SARS-CoV-2. *N Engl J Med* **383**, 590-592 (2020).
50. Mendez, D., *et al.* ChEMBL: towards direct deposition of bioassay data. *Nucleic Acids Res* **47**, D930-d940 (2019).
51. Shabalin, A.A. Matrix eQTL: ultra fast eQTL analysis via large matrix operations. *Bioinformatics* **28**, 1353-1358 (2012).
52. Rohloff, J.C., *et al.* Nucleic Acid Ligands With Protein-like Side Chains: Modified Aptamers and Their Use as Diagnostic and Therapeutic Agents. *Mol Ther Nucleic Acids* **3**, e201 (2014).
53. Gold, L., *et al.* Aptamer-based multiplexed proteomic technology for biomarker discovery. *PLoS One* **5**, e15004 (2010).
54. Chapman, A.B., *et al.* A Natural Language Processing System for National COVID-19 Surveillance in the US Department of Veterans Affairs. (2020).
55. Hunter-Zinck, H., *et al.* Genotyping Array Design and Data Quality Control in the Million Veteran Program. *Am J Hum Genet* **106**, 535-548 (2020).
56. Willer, C.J., Li, Y. & Abecasis, G.R. METAL: fast and efficient meta-analysis of genomewide association scans. *Bioinformatics* **26**, 2190-2191 (2010).
57. Giambartolomei, C., *et al.* A Bayesian framework for multiple trait colocalization from summary association statistics. *Bioinformatics* **34**, 2538-2545 (2018).
58. Lundberg, M., Eriksson, A., Tran, B., Assarsson, E. & Fredriksson, S. Homogeneous antibody-based proximity extension assays provide sensitive and specific detection of low-abundant proteins in human blood. *Nucleic Acids Res* **39**, e102 (2011).
59. Olink Target 96 & Target 48 panels for protein biomarker discovery.
60. Yu, G., Wang, L.G., Han, Y. & He, Q.Y. clusterProfiler: an R package for comparing biological themes among gene clusters. *Omics* **16**, 284-287 (2012).

Author contribution

J.P.C., A.S.B. and J.M.G. conceived the study design. A.G., A.P.B. and A.R.L. defined the actionable genome, and identified and curated drug information relating to SARS-CoV-2; P.B. and I.B.-H. provided biological annotation relating to SARS-CoV-2; C.G. performed stepwise conditional analysis on GTEx raw data; D.P. tested associations for COVID-19 in MVP; L.G. and J.H.Z. performed meta-analysis of HGI and MVP; L.G. performed Mendelian randomization analysis; L.G. and C.G. performed colocalization analyses; L.G. and B.P.P. performed conditional analysis on Olink proteins; L.G. and E.A. performed phenome-wide scans; A.C.P. performed pathway enrichment analysis; J.N.D., A.S.B., and J.E.P. provided INTERVAL data; Several authors were involved in the curation of the MVP data; L.G., C.G., A.C.P., A.G., D.P., A.S.B. and J.P.C. wrote the manuscript. J.P.C. oversaw all analyses. All authors critically reviewed the manuscript.

Competing interests

The authors declare no competing interests.

Figure Legends

Figure 1. **Outline of the analyses performed**. Using multiple data sources, this study tested *cis*-pQTL and *cis*-eQTL proposed instruments for actionable druggable proteins against COVID-19 hospitalization summary statistics meta-analyzed from the Host Genetics Initiative and the Million Veteran Program. Significant MR associations that also showed evidence for colocalization were investigated further with an independent platform (Olink), phenome-wide scans of relevant variants, and pathway enrichment.

Figure 2. Manhattan plot of results from actionable druggable genome-wide Mendelian randomization analysis. Mendelian randomization estimates were calculated using inverse-variance weighting and fixed effects for instruments that contained more than one variant, and Wald-ratio for instruments with one variant. Blue solid line indicates the *P* value threshold for significance ($P<3.96\times10^{-5}$, 0.05 Bonferroni-corrected for 1,263 actionable druggable genes) and red dashed line indicates a suggestive ($P<5.00\times10^{-4}$) threshold. Genes are labeled by their most significant MR association. For example, the results for *IL10RB* is most significant with *cis*-eQTL proposed instruments derived in skeletal muscle tissue ($P=2.31\text{x}10^{-14}$), which is the point labeled. Results are plotted by the gene start position. All MR results with *P* value less than 5.00×10^{-4} used the GTEx *cis*-eQTLs as proposed instruments.

Figure 3. Genomic context, local association plot and LD structure of the *IFNAR2/IL10RB* region. a, Local association plot (*N*=1,377,758) of the interval defined by all unique eQTLs for *IL10RB* or *IFNAR2*. Color code represents the degree of linkage disequilibrium with the most associated marker in 1000G Europeans. **b,** Genomic context of the region. Coding genes are

represented by the refseq transcript. Bars represent epigenome Roadmap layered H3K27 acetylation markers. Connecting lines represent significant Hi-C interactions. **c,** Set of rsIDs used as proposed instruments for Mendelian Randomization analysis. Color code represents instruments for *IL10RB* (blue circles), *IFNAR2* (green circles). Orange half-circles represent pQTLs for IL-10RB. **d,** Linkage disequilibrium structure and blocks defined using European populations from 1000G project.

Figure 4. **Regional association plots of the *IFNAR2-IL10RB* locus**. Regional association plots for **a,** *IL10RB* gene expression in tibial nerve tissue from GTEx (*N*=532), **b,** COVID-19 hospitalization from HGI and MVP trans-ancestry meta-analysis (*N*=1,377,758) **c, d,** Vascular endothelial growth factor receptor 2 (VEGFR2) and tryptase gamma (TPSG1), respectively, measured by SomaLogic in 3,301 INTERVAL participants. All show the correlation (1000G European ancestry) for rs13050728, the *cis*-eQTL most associated with COVID-19 hospitalization in the *IL10RB-IFNAR2* region. All colocalize with each other (PP.H4>0.96 for all).

760 Table 1. Significant ($P<3.96\times10^{-5}$) MR results.

Gene	Tissue	beta	S.E.	*P* value	P_{het}	Variants in instrument	Colocalization
IL10RB	Muscle Skeletal	0.5078	0.0665	2.31E-14	0.9732	rs2300370, rs2834167	0.98, <0.01
IL10RB	Nerve Tibial	0.2859	0.0384	9.76E-14	0.0052	rs13050728, rs2834167, rs2266590	0.98, <0.01, <0.01
CCR1	Cells Cultured fibroblasts	0.4449	0.0612	3.60E-13	NA	rs13095940	<0.01
IL10RB	Brain Nucleus accumbens basal ganglia	0.2541	0.0363	2.58E-12	0.0019	rs2834167, rs17860115	0.75, 0.98
IL10RB	Brain Caudate basal ganglia	0.2635	0.0398	3.61E-11	0.0003	rs2834167, rs1051393	0.01, 0.97
IFNAR2	Muscle Skeletal	0.5881	0.0909	9.75E-11	NA	rs2300370	0.98
IL10RB	Brain Cerebellar Hemisphere	0.1405	0.0229	8.22E-10	0.0389	rs2834167, rs2236758	0.01, 0.95
IL10RB	Breast Mammary Tissue	0.6490	0.1079	1.82E-09	NA	rs12053666	0.95
IL10RB	Brain Frontal Cortex BA9	0.4667	0.0790	3.55E-09	0.0366	rs2834167, rs1131668	0.14, 0.97
IL10RB	Brain Cortex	0.1929	0.0328	3.99E-09	0.0354	rs2834167, rs1131668	0.02, 0.96
CCR1	Esophagus Gastroesophageal Junction	0.1776	0.0302	4.11E-09	NA	rs13059906	0.05
IL10RB	Brain Cerebellum	0.1147	0.0197	5.82E-09	0.0239	rs2834167, rs1131668	<0.01, 0.96
CCR1	Esophagus Mucosa	0.4338	0.0751	7.60E-09	NA	rs34059564	<0.01
IFNAR2	Esophagus Mucosa	-0.4883	0.0865	1.63E-08	NA	rs11911133	0.92
PDE4A	Artery Aorta	-0.5420	0.0965	1.98E-08	0.0202	rs370630099, rs45524632	0.41, 0.61
IL10RB	Testis	0.7104	0.1364	1.92E-07	NA	rs2284550	0.11
IFNAR2	Skin not Sun Exposed Suprapubic	-0.3360	0.0671	5.46E-07	NA	rs8127500	<0.01
IFNAR2	Pancreas	-0.4708	0.0957	8.63E-07	NA	rs1476415	0.06
ACE2	Brain Frontal Cortex BA9	0.1121	0.0233	1.56E-06	NA	rs4830976	0.95
IFNAR2	Cells Cultured fibroblasts	-0.3893	0.0819	1.98E-06	NA	rs1131668	0.92
IL10RB	Cells Cultured fibroblasts	-0.5197	0.1093	1.98E-06	NA	rs1131668	0.96
CCR5	Lung	-0.5868	0.1272	3.99E-06	NA	rs12639314	0.02
IL10RB	Esophagus Gastroesophageal Junction	0.4678	0.1052	8.80E-06	NA	rs56079299	0.96

Significant Mendelian randomization results, $P<3.96\times10^{-5}$ (0.05 Bonferroni-corrected for 1,263 actionable druggable genes). Mendelian randomization estimates were calculated using inverse-variance weighting and fixed effects for instruments that contained more than one variant, and Wald-ratio for instruments with one variant. All results used *cis*-eQTL instruments and no results using *cis*-pQTL instruments yielded results $P<3.96\times10^{-5}$. P_{het} refers to the heterogeneity *P* value across individual-variant MR estimates within a genetic instrument calculated using the Cochrane Q method, therefore instruments containing one variant were not tested for heterogeneity. A positive beta estimate indicates that more gene expression is associated with higher risk of COVID-19 hospitalization. "Colocalization" indicates PP.H4 between eQTLs and COVID-19 hospitalization. For example, for IL10RB in skeletal muscle, the primary GWAS with rs2300370 as the peak *cis*-eQTL colocalizes with COVID-19 hospitalization at PP.H4=0.98, and the secondary GWAS (i.e. after adjusting for rs2300370) with rs2834167 as the peak *cis*-eQTL does not colocalize with COVID-19 hospitalization (PP.H4<0.01).

METHODS

Identification of actionable druggable genes suitable for repurposing against COVID-19

Information about drugs and clinical candidates, and their therapeutic targets, was obtained from the ChEMBL database (release 26[50], **Supplementary Methods**). For the purposes of our COVID-19 drug repurposing efforts, actionable proteins were defined as those that are therapeutic targets of approved drugs and clinical candidates or are potential targets of approved drugs. Therapeutic targets were identified from the drug mechanism of action information in ChEMBL and linked to their component proteins. Each protein was assigned a confidence level based on the type and size of target annotated, and the resulting list was filtered to remove non-human proteins and those with lower confidence assignments (cases where the therapeutic target consists of more than 10 proteins or the protein is known to be a non-drug-binding subunit of a protein complex). For approved drugs, additional potential human target proteins were identified from pharmacological assay data in ChEMBL with recorded affinity/efficacy measurements <= 100nM (represented by a pChEMBL value >= 7).

A total of 1,263 unique human proteins were identified as 'actionable' from data available in ChEMBL. These consisted of 531 proteins that are therapeutic targets of approved drugs, 381 additional proteins that are therapeutic targets of clinical candidates and 351 additional proteins that are bound by approved drugs, but not annotated as the therapeutic targets. While the biological relevance of the latter group of targets in the context of the approved drug indications may be unclear, the high affinity/efficacy measurements suggest the drug should be capable of modulating these proteins, should they be found to be relevant to COVID-19 (although likely not in a selective manner). Proteins were further annotated with biological and drug information

relating to their potential role in SARS-CoV-2 infection (**Supplementary methods**) such as change in abundance during infection, interaction with viral proteins or the activity of drugs in antiviral cell-based assays. Of the 1,263 actionable proteins identified previously, 300 were annotated as biologically relevant in SARS-CoV-2 infection and 547 were targets of drugs with some evidence of COVID-19 relevance from cell-based assays, clinical trials or the ATC classification (**Supplementary Table 2**).

Selection of proposed instruments

eQTL proposed instruments

We proposed eQTL instruments using raw data from GTEx Version 8 by performing conditional analysis on normalized gene expression in European ancestry individuals in 49 tissues that had at least 70 samples. eQTLs were derived in all 49 tissues (i.e. we did not restrict it to tissues we thought most relevant to COVID-19) because the biological relevance of tissues to SARS-CoV-2 infection is still rapidly evolving. We used Matrix eQTL[51] and followed the same procedure as outlined by the GTEx consortium (https://gtexportal.org/home/). Briefly, after filtering the genotypes (genotype missingness <0.05, MAF<0.01, HWE<0.000001, removing ambiguous SNPs), within each tissue, we performed GWAS between variants and gene expression adjusting for sex, the first 5 principal components of European genetic ancestry, PEER factors, sequencing platform and protocol. To identify independent eQTLs, we performed conditional analysis in regions around associations that fell below genome-wide significance, additionally adjusting for the peak variant if there exists an association reaching a *P*-value of 5.00×10^{-8}. *Cis*-eQTLs were defined as significant ($P<5.00\times10^{-8}$) associations within 1Mb on either side of the encoded gene. To convert from build 38 to build 37, we used the table available from the GTEx consortium for

all variants genotyped in GTEx v8 and hg19 liftover, (https://storage.googleapis.com/gtex_analysis_v8/reference/GTEx_Analysis_2017-06-05_v8_WholeGenomeSeq_838Indiv_Analysis_Freeze.lookup_table.txt.gz). In each tissue, multiple GW-significant ($P<5.00\times10\text{-}8$) eQTLs for the same gene were combined into a single instrument using inverse-variance weighting and fixed-effects meta-analysis across variant-level MR estimates for each variant, a standard two-sample MR approach. For example, for IL10RB expression in skeletal muscle tissue, there were two conditionally-independent eQTLs (rs2300370 and rs2834167, Table 1); a variant-level MR-estimate was obtained for each by dividing the beta-coefficient for COVID-19 hospitalization by the beta-coefficient of the eQTL, and dividing the standard error of the COVID-19 hospitalization estimate by the beta-coefficient of the eQTL. The two variant-level MR estimates were then meta-analyzed using inverse-variance weighting and fixed effects to yield the final MR result. Instruments for expression of the same gene derived in different tissues were tested separately.

pQTL proposed instruments

We proposed pQTL instruments from two sources of publicly available data that reported conditionally independent pQTLs for proteins measured by the SomaLogic Inc. (Boulder, Colorado, US) SomaScan[52,53] platform: (1) Sun *et al.*[13], which reported results for 2,994 proteins in 3,301 INTERVAL participants and (2) Pietzner *et al.*[14], which reported results for 179 proteins in 10,708 participants of the Fenland cohort. In both, we restricted proposed instrumental variants to *cis*-pQTLs for actionable proteins, used a *P* value threshold of 5×10^{-8} and removed variants with MAF<0.01. MR was run independently for each data source (i.e.

proposed instruments for the same protein in different platforms were tested against COVID-19 hospitalization independently).

Estimates for COVID-19 hospitalization

To generate outcome summary-statistics, we meta-analyzed results from the Million Veteran Program (MVP), an ongoing, prospective cohort recruiting from 63 Veterans Health Administration (VA) medical facilities (**Supplementary Methods)**, and the Host Genetics Initiative,[9] a global collaboration to accumulate GWAS on COVID-19 infection and clinical manifestations.

In MVP, 1,062 COVID-19 cases (**Supplementary Table 1)** were identified between March 1st and September 17, 2020 using an algorithm developed by the VA COVID National Surveillance Tool (NST). The NST classified COVID-19 cases as positive or negative based on reverse transcription polymerase chain reaction (rRT-PCR) laboratory test results conducted at VA clinics, supplemented with Natural Language Processing (NLP) on clinical documents. The algorithm to identify COVID-19 patients is continually updated to ensure new annotations of COVID-19 are captured from the clinical notes, with chart reviews performed periodically to validate the algorithm.[54] COVID-19-related hospitalizations were defined as admissions from 7 days before up to 30 days after a patient's first positive test for SARS-CoV-2 test. We tested association between all our proposed genetic instruments and COVID-19 hospitalization (versus population controls) in MVP adjusting for age, sex and the first 10 principal components in three mutually-exclusive, ancestry-specific strata separately (European, African and Hispanic ancestry) using PLINK v2 (analysis completed on October 10, 2020). We have previously provided a detailed description of the genotype data quality control process[55]. The MVP received

865 ethical and study protocol approval by the Veterans Affairs Central Institutional Review Board
866 and informed consent was obtained for all participants.
867
868 We downloaded publicly available summary statistics for the B2 outcome from Host Genetic
869 Initiative on October 4, 2020 (release 4 version 1). In total, HGI accumulated 6,492 cases of
870 COVID-19 hospitalization through collaboration from 16 contributing studies (**Supplementary**
871 **Table 1**), which were asked to define cases as "hospitalized laboratory confirmed SARS-CoV-2
872 infection (RNA and/or serology based), hospitalization due to corona-related symptoms" versus
873 population controls
874 (https://docs.google.com/document/d/1okamrqYmJfa35ClLvCt_vEe4PkvrTwggHq7T3jbeyCI/vi
875 ew) and use a model that adjusts for age, age^2, sex, age*sex, PCs, and study specific covariates
876 (https://docs.google.com/document/d/16ethjgi4MzlQeO0KAW_yDYyUHdB9kKbtfuGW4XYV
877 KQg/view). Summary statistics (i.e. betas and standard errors) from the four analyses, MVP-
878 European, MVP-African, MVP-Hispanic, and COVID-19 Host Genetics Initiative (HGI
879 summary statistics were already meta-analyzed from GWAS that contributed to the HGI
880 consortium) were meta-analyzed using METAL software[56] with inverse-variance weighting and
881 fixed effects.
882
883 Quantile-Quantile plots of *P* values from genome-wide association testing in MVP did not
884 display any inflation of results in any ancestry-specific stratum (**Supplementary Figure 1**).
885 Additionally, P_{het} values from the meta-analysis (output from METAL's "analyze heterogeneity"
886 command) were not inflated (**Supplementary Figure 2**), indicating that there is little overall
887 heterogeneity between estimates across ancestries within MVP and between MVP and HGI.
888

889 **Mendelian randomization and colocalization**

890 We conducted MR analyses using the R package TwoSampleMR
891 (https://mrcieu.github.io/TwoSampleMR/). We used fixed-effects, inverse-variance weighted
892 MR for proposed instruments that contain more than one variant, and Wald-ratio for proposed
893 instruments with one variant. For proposed instruments with multiple variants, we also tested the
894 heterogeneity across variant-level MR estimates, using the Cochrane Q method
895 (mr_heterogeneity option in TwoSampleMR package). We defined significant MR results using
896 a *P* value threshold of $P<3.96\times10^{-5}$ (0.05 Bonferroni-corrected for 1,263 actionable druggable
897 genes) and identified a list of "suggestive" actionable druggable targets that passed a threshold of
898 $P<5.00\times10^{-4}$. For statistically significant MR results, we also performed colocalization[57] between
899 each eQTL and the trans-ancestry meta-analysis on COVID-19 hospitalization using the moloc R
900 package (https://github.com/clagiamba/moloc) with default priors (probability of shared causal
901 variant for trait 1 and trait 2 is $p1=p2=1\times10^{-4}$, probability of shared causal variant across two
902 traits is $p12=1\times10^{-5}$). For example, if a proposed instrument contained two variants, we
903 performed colocalization for the primary eQTL GWAS with COVID-19 hospitalization, as well
904 as the secondary eQTL GWAS (i.e. eQTL GWAS after adjusting for peak variant from primary
905 GWAS) with COVID-19 hospitalization. Statistically significant MR hits with posterior
906 probability for hypothesis-4 (PP.H4) > 0.8 (i.e. the probability of a shared causal variant) for a
907 least one instrumental variant were then investigated further using the following analyses.
908

909 **Identifying pQTLs using Olink assay**

910 We performed stepwise conditional analysis to identify *cis*-pQTL proposed instruments for
911 proteins that passed our significance and colocalization thresholds and were one of 354 unique

912 proteins measured on four Olink[58] panels (CVD1, CVD2, Inflammation, and Neuro[59]) in 4,998
913 INTERVAL participants.[13] INTERVAL is a prospective cohort study of ~50,000 blood donors
914 recruited from 25 National Health Service Blood and Transplant centers in England. Participants
915 were genotyped using the UK Biobank Affymetrix Axiom array, followed by phasing using
916 SHAPEIT3 and imputation on the Sanger Imputation Server using a 1000 Genomes Phase 3-
917 UK10K imputation panel. Alleles were tested against Olink proteins using SNPTEST v2.5.2 and
918 adjusted for age, sex, plate, time from blood draw to processing, season and the first 5 principal
919 components. Conditional analysis was performed by adjusting for peak variants until no
920 association fell below 5.00×10^{-6}.
921
922 **Phenome-wide scan**
923 We conducted a phenome-wide scan for variants with the following goals. First, we want to
924 evaluate that our proposed instruments could reproduce the known phenotype associations (e.g.
925 disease, biomarkers) ascribed to the drug that are due to on-target effects. Secondly, we want to
926 identify if our proposed instruments are associated with comorbidities associated with greater
927 likelihood of SARS-CoV-2 testing or predictors of hospitalization in COVID-19 patients, as this
928 could potentially highlight the presence of certain biases.[21] Also, for genes that were the target of
929 licensed drugs, we checked whether the disease indication was also a risk factor for COVID-19
930 outcomes, as this might introduce a bias analogous to confounding by indication in MR.
931
932 To accomplish these goals, we investigated proposed instruments for associations of a phenome-
933 wide range of outcomes. We searched the GTEx[12] Portal (https://gtexportal.org/home/) for gene
934 expression, and Phenoscanner[17] (http://www.phenoscanner.medschl.cam.ac.uk/) for proteins,

935 traits and diseases. We additionally queried variants in GWAS for 354 Olink proteins (described
936 earlier), and all the proteins measured by the SomaScan platform (described in Sun *et al.*[13]) in
937 3,301 INTERVAL participants.
938
939 **Characterizing downstream transcriptional consequences of associated loci**
940 In order to confirm the specificity of the identified loci and to better explore their most important
941 downstream transcriptional consequences, we have studied the transcriptional landscape
942 modulation associ3ated with the selected variants using GTEx V8 data with representation of 49
943 different tissues. For this we have used rs13050728 as the proxy of the *IFNAR2*/*IL10RB* locus
944 and rs4830976 as the proxy of the *ACE2* locus and conducted a differential gene-expression
945 analysis for all transcripts available in GTEx V8. After fitting models for all genes, enrichment
946 pathway analysis was conducted to retrieve the most enriched pathways using both the
947 differentially expressed (DE) gene list (through an over-representation analysis) and a Gene Set
948 Enrichment Analysis framework (using the R package clusterProfiler[60]). For enrichment
949 analysis we have used the corpus from WikiPathways, Gene Ontology and Reactome.
950 **Data availability**
951 GTEx project version 8 data are available at: https://gtexportal.org/home/. CheMBL database
952 data are available at: https://www.ebi.ac.uk/chembl/. Fenland-Somalogic protein GWAS data are
953 available at: https://omicscience.org/apps/covidpgwas/. Host Genetics Initiative COVID-19
954 hospitalization summary statistics are available at: https://www.covid19hg.org/. PhenoScanner
955 results are available at http://www.phenoscanner.medschl.cam.ac.uk/.
956

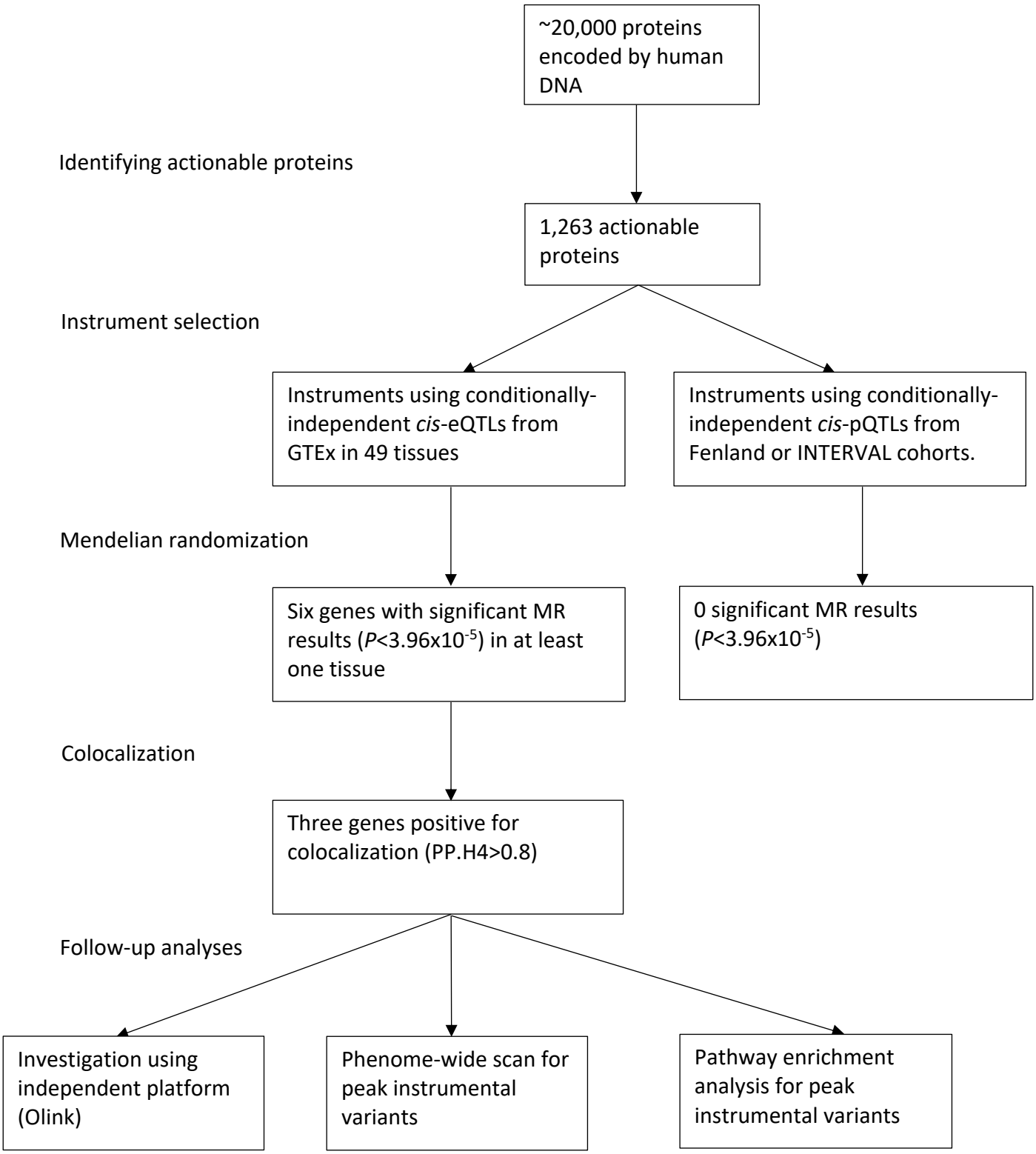
~20,000 proteins encoded by human DNA
Identifying actionable proteins
1,263 actionable proteins
Instrument selection
Instruments using conditionally-independent *cis*-eQTLs from GTEx in 49 tissues
Instruments using conditionally-independent *cis*-pQTLs from Fenland or INTERVAL cohorts.
Mendelian randomization
Six genes with significant MR results (P<3.96x10^{-5}) in at least one tissue
0 significant MR results (P<3.96x10^{-5})
Colocalization
Three genes positive for colocalization (PP.H4>0.8)
Follow-up analyses
Investigation using independent platform (Olink)
Phenome-wide scan for peak instrumental variants
Pathway enrichment analysis for peak instrumental variants

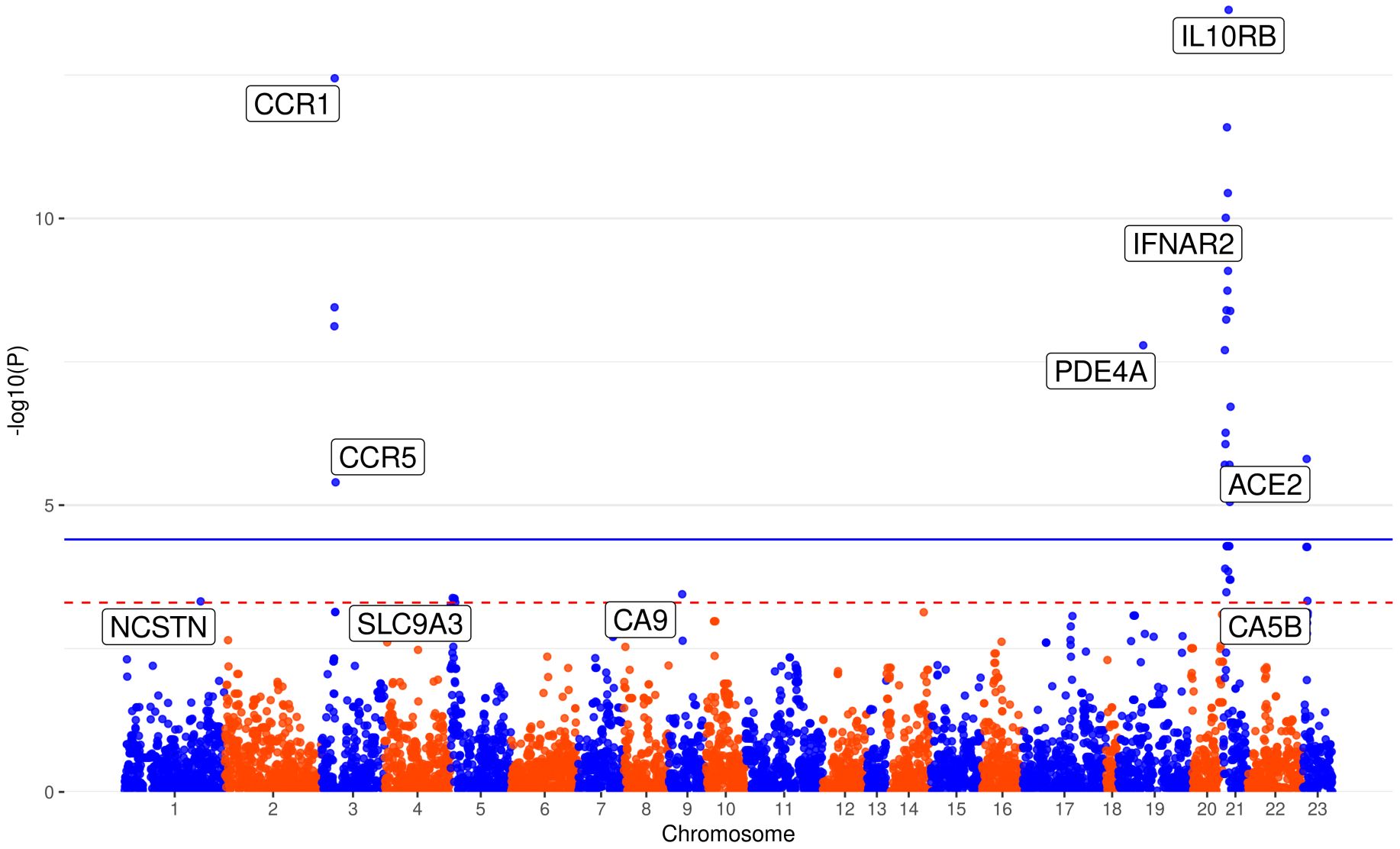
IL10RB
CCR1
IFNAR2
PDE4A
CCR5
ACE2
NCSTN
SLC9A3
CA9
CA5B
-log10(P)
10
5
0
1
2
3
4
5
6
7
8
9
10
11
12
13
14
15
16
17
18
19
20
21
22
23
Chromosome

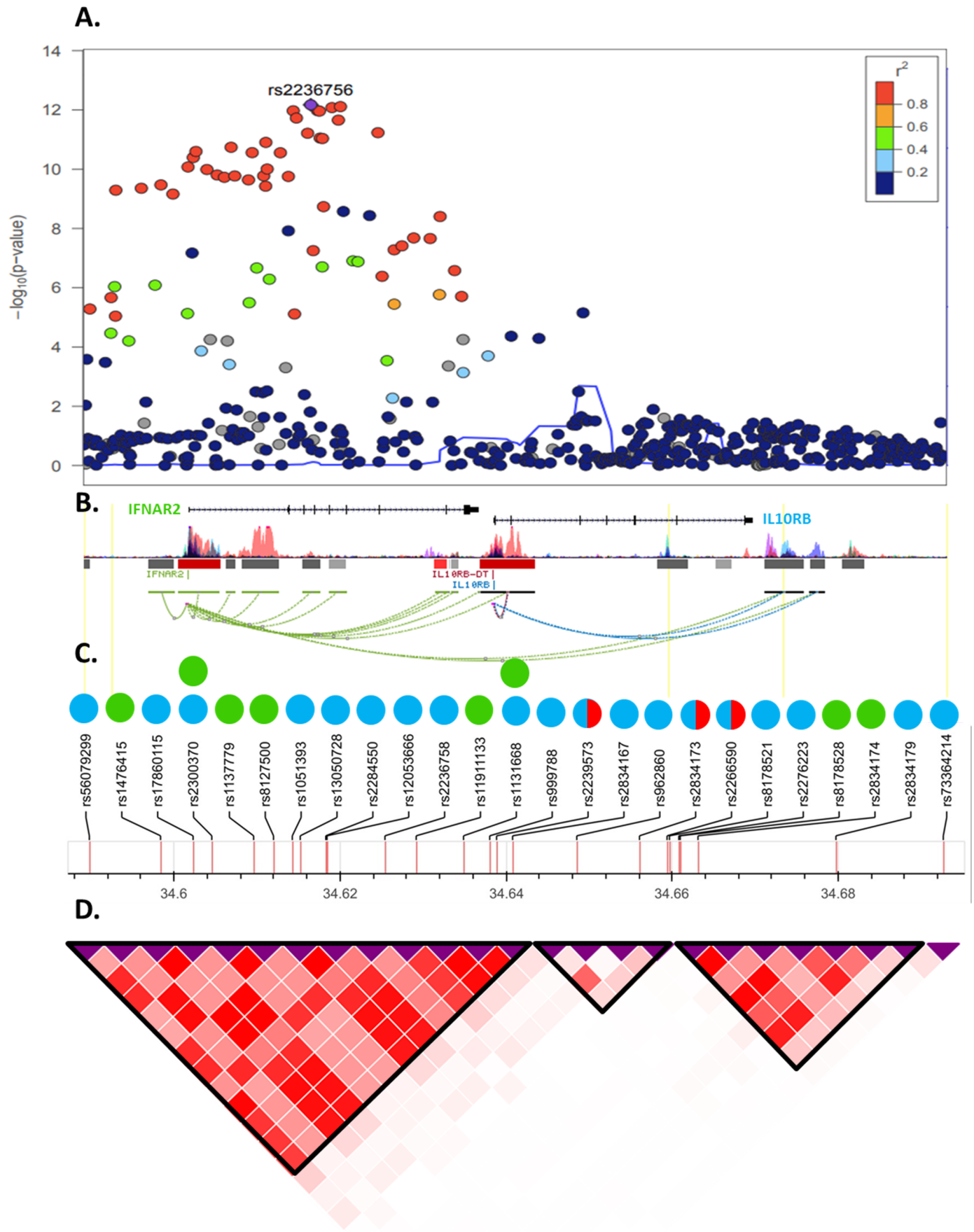
A.
rs2236756
r²
0.8
0.6
0.4
0.2
−log10(p−value)
14
12
10
8
6
4
2
0
B.
IFNAR2
IL10RB
IFNAR2
IL10RB-DT
IL10RB
C.
rs56079299
rs1476415
rs17860115
rs2300370
rs1137779
rs8127500
rs1051393
rs13050728
rs2284550
rs12053666
rs2236758
rs11911133
rs1131668
rs999788
rs2239573
rs2834167
rs962860
rs2834173
rs2266590
rs8178521
rs2276223
rs8178528
rs2834174
rs2834179
rs73364214
34.6
34.62
34.64
34.66
34.68
D.

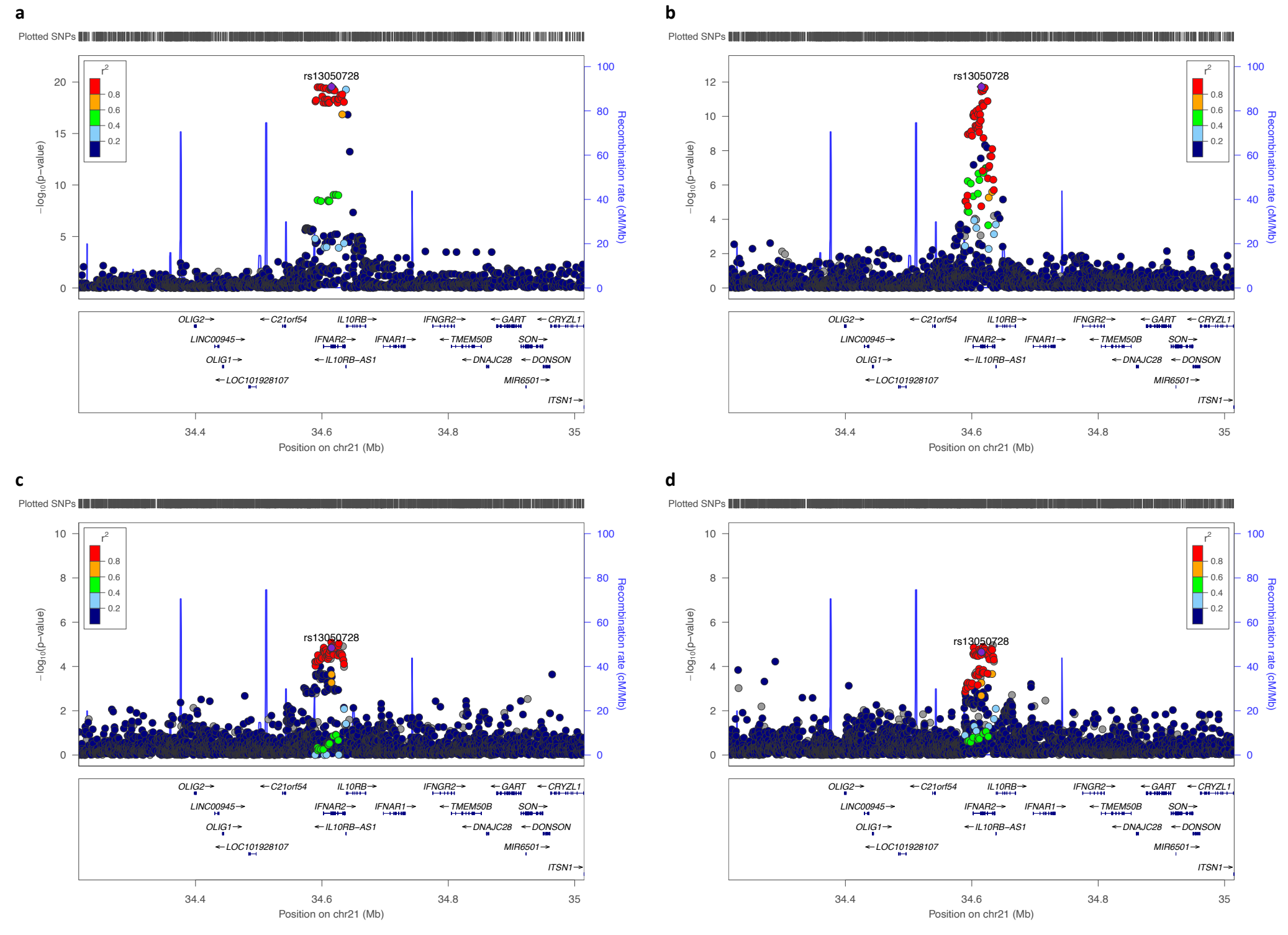
a
b
c
d
Plotted SNPs
rs13050728
r²
0.8
0.6
0.4
0.2
−log10(p−value)
Recombination rate (cM/Mb)
OLIG2→
←C21orf54
IL10RB→
IFNGR2→
←GART
←CRYZL1
LINC00945→
IFNAR2→
IFNAR1→
←TMEM50B
SON→
OLIG1→
←IL10RB−AS1
←DNAJC28
←DONSON
←LOC101928107
MIR6501→
ITSN1→
34.4
34.6
34.8
35
Position on chr21 (Mb)

a

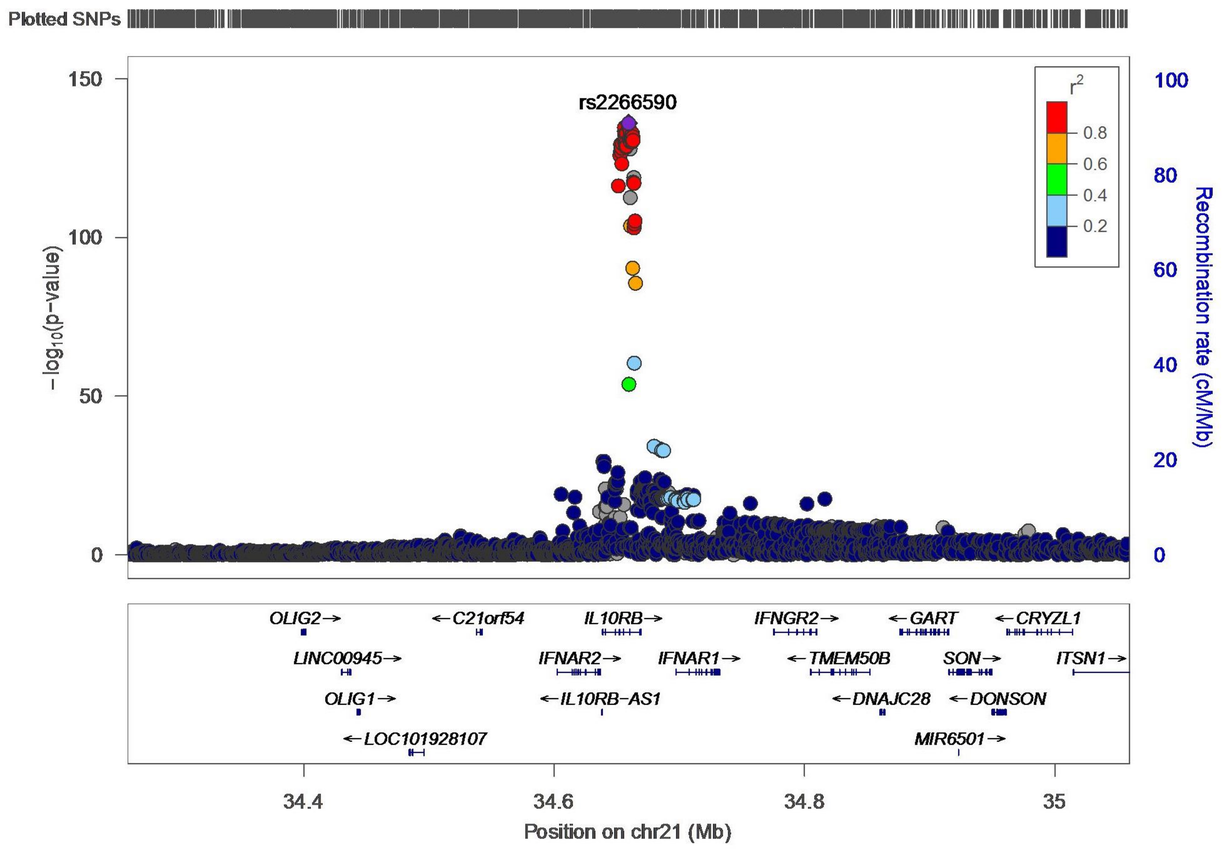
Plotted SNPs
rs2266590
r2
0.8
0.6
0.4
0.2
−log10(p−value)
Recombination rate (cM/Mb)
OLIG2→ ←C21orf54 IL10RB→ IFNGR2→ ←GART ←CRYZL1
LINC00945→ IFNAR2→ IFNAR1→ ←TMEM50B SON→ ITSN1→
OLIG1→ ←IL10RB−AS1 ←DNAJC28 ←DONSON
←LOC101928107 MIR6501→
Position on chr21 (Mb)

b

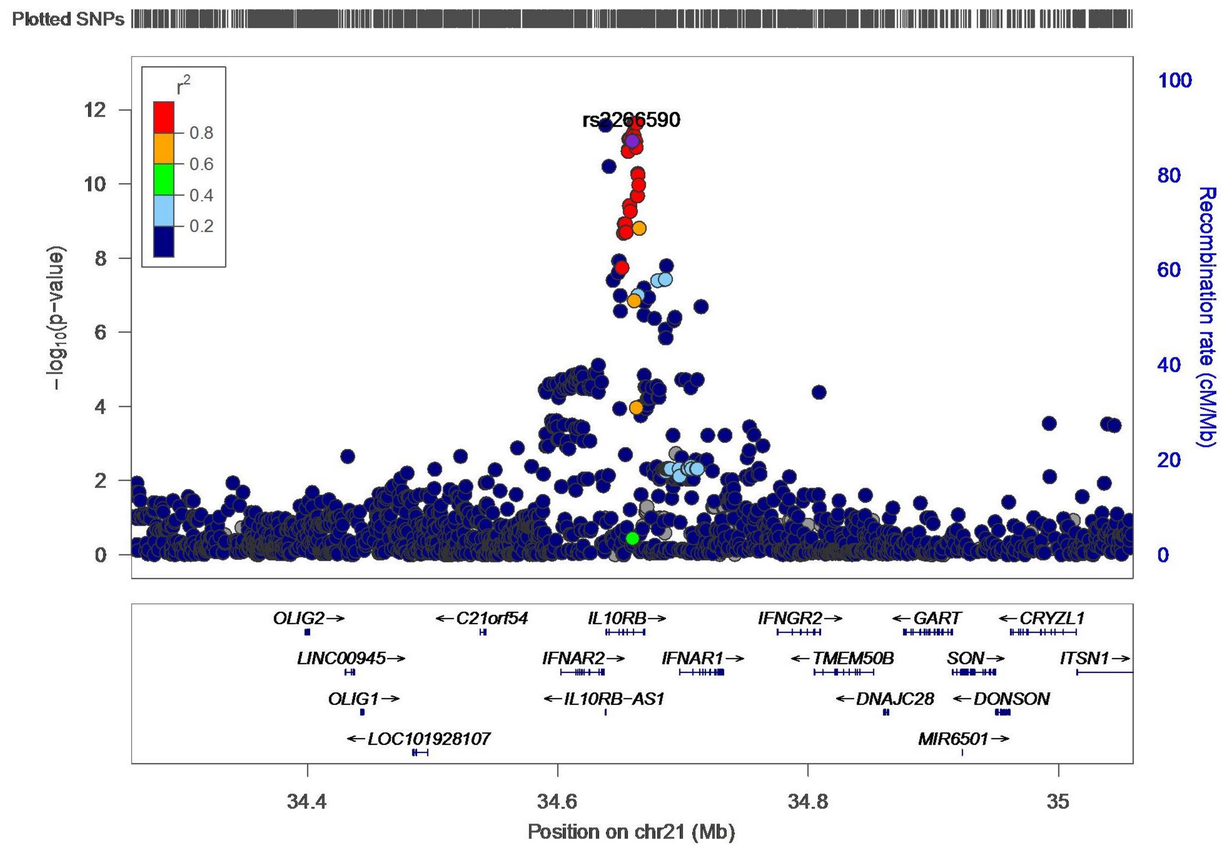
Plotted SNPs
rs2266590
r2
0.8
0.6
0.4
0.2
−log10(p−value)
Recombination rate (cM/Mb)
OLIG2→ ←C21orf54 IL10RB→ IFNGR2→ ←GART ←CRYZL1
LINC00945→ IFNAR2→ IFNAR1→ ←TMEM50B SON→ ITSN1→
OLIG1→ ←IL10RB−AS1 ←DNAJC28 ←DONSON
←LOC101928107 MIR6501→
Position on chr21 (Mb)

c

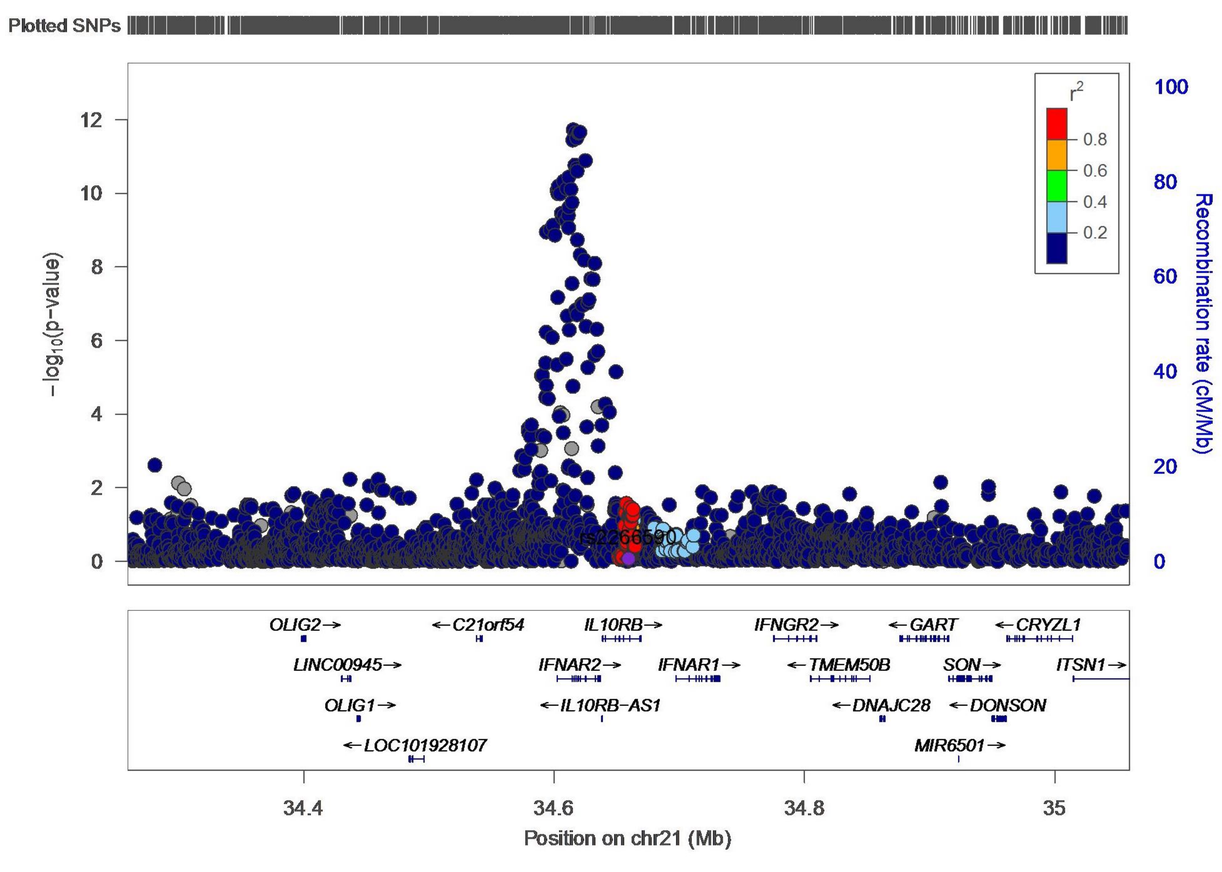
Plotted SNPs
rs2266590
r2
0.8
0.6
0.4
0.2
−log10(p−value)
Recombination rate (cM/Mb)
OLIG2→ ←C21orf54 IL10RB→ IFNGR2→ ←GART ←CRYZL1
LINC00945→ IFNAR2→ IFNAR1→ ←TMEM50B SON→ ITSN1→
OLIG1→ ←IL10RB−AS1 ←DNAJC28 ←DONSON
←LOC101928107 MIR6501→
Position on chr21 (Mb)

d

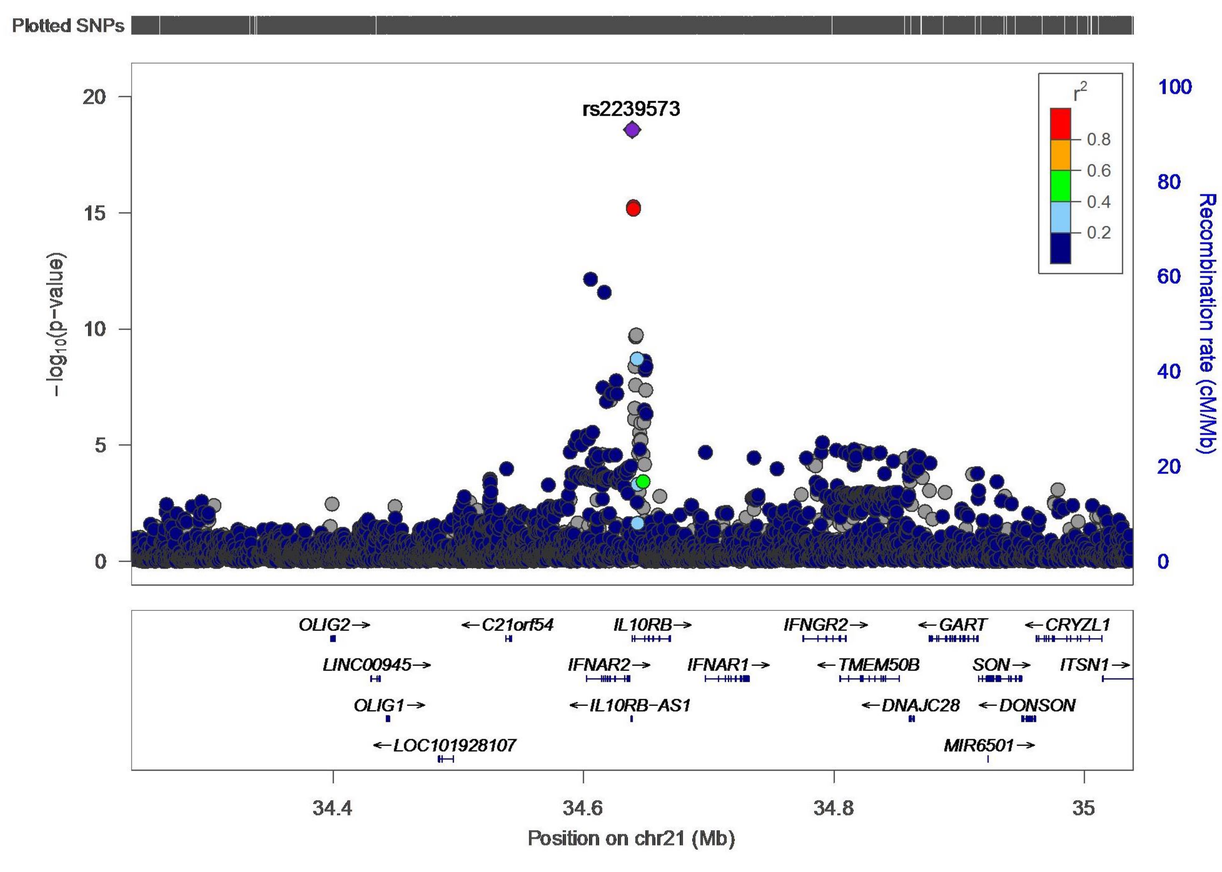
Plotted SNPs
rs2239573
r2
0.8
0.6
0.4
0.2
−log10(p−value)
Recombination rate (cM/Mb)
OLIG2→ ←C21orf54 IL10RB→ IFNGR2→ ←GART ←CRYZL1
LINC00945→ IFNAR2→ IFNAR1→ ←TMEM50B SON→ ITSN1→
OLIG1→ ←IL10RB−AS1 ←DNAJC28 ←DONSON
←LOC101928107 MIR6501→
Position on chr21 (Mb)

e

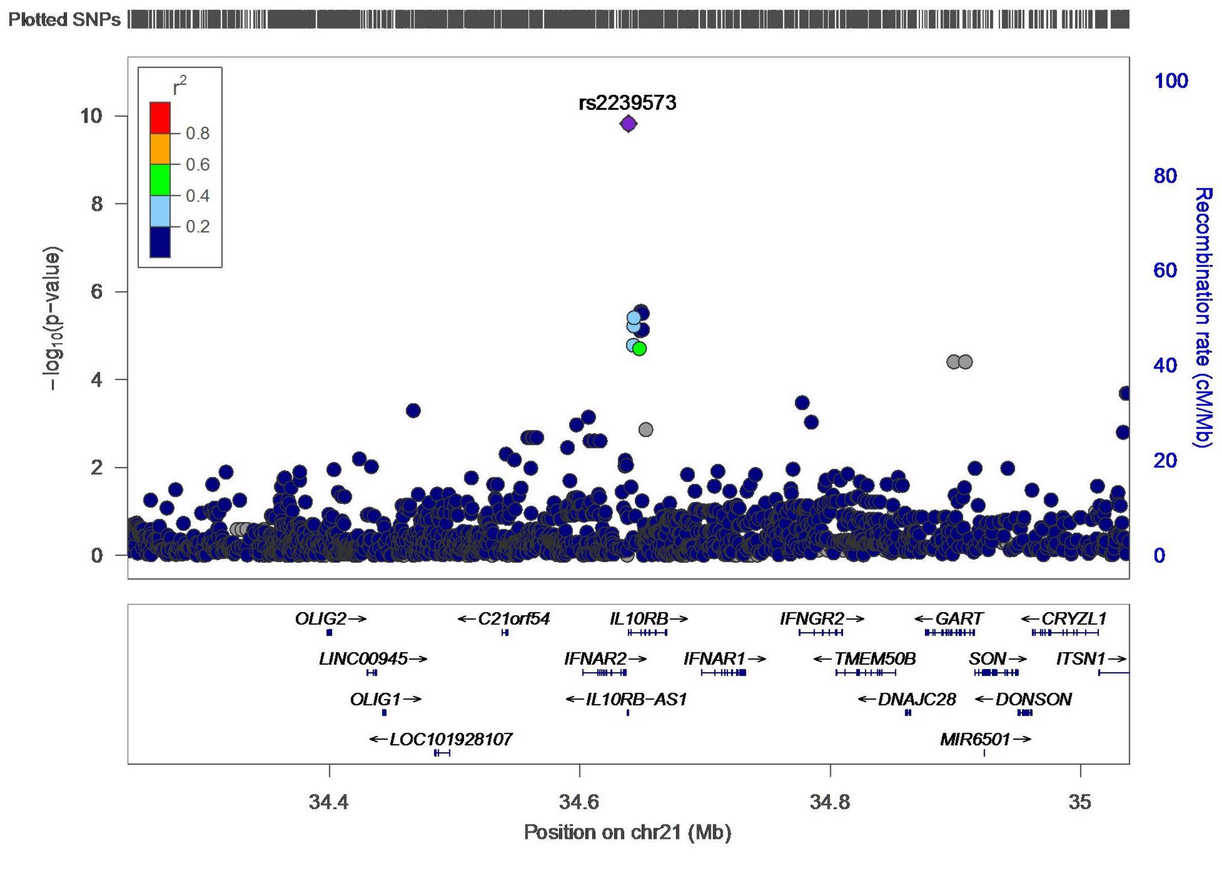
Plotted SNPs
rs2239573
r2
0.8
0.6
0.4
0.2
−log10(p−value)
Recombination rate (cM/Mb)
OLIG2→ ←C21orf54 IL10RB→ IFNGR2→ ←GART ←CRYZL1
LINC00945→ IFNAR2→ IFNAR1→ ←TMEM50B SON→ ITSN1→
OLIG1→ ←IL10RB−AS1 ←DNAJC28 ←DONSON
←LOC101928107 MIR6501→
Position on chr21 (Mb)

f

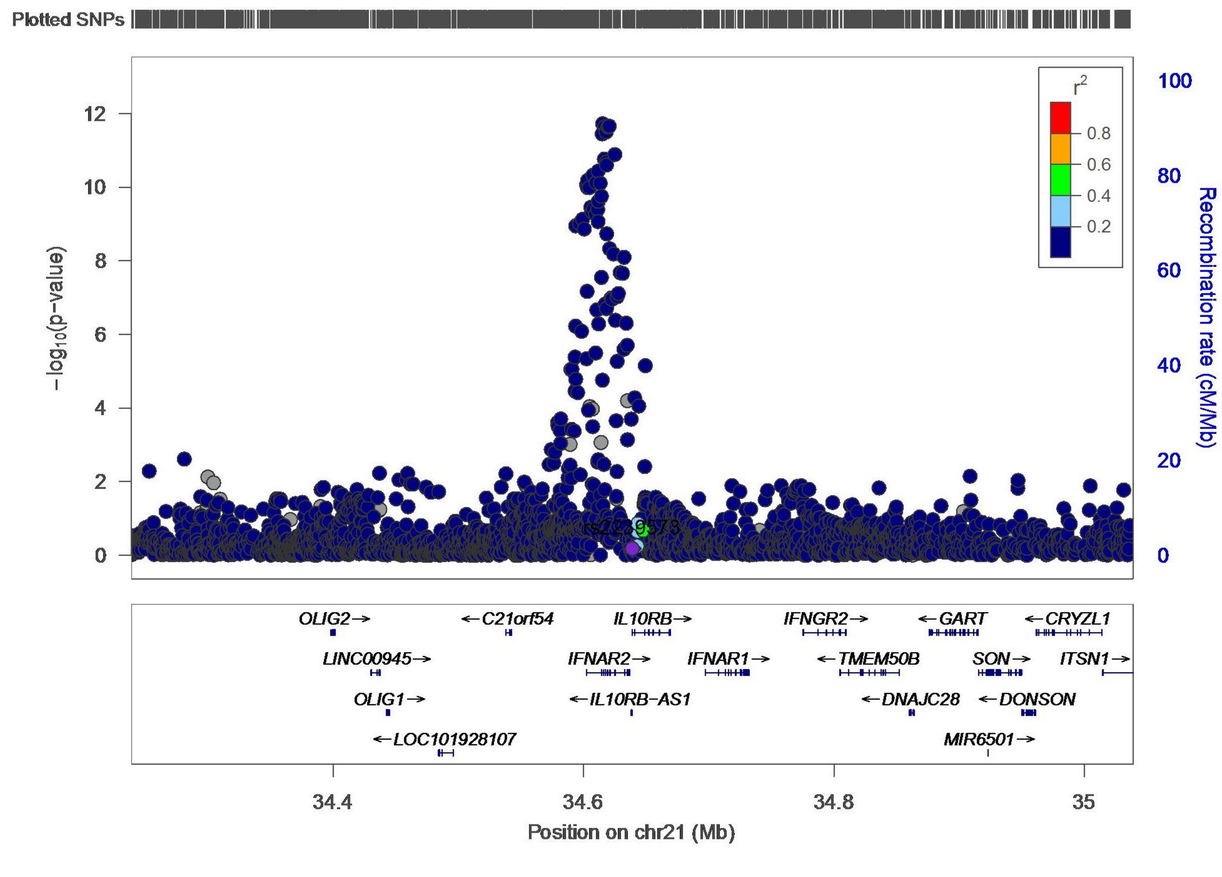
Plotted SNPs
rs2239573
r2
0.8
0.6
0.4
0.2
−log10(p−value)
Recombination rate (cM/Mb)
OLIG2→ ←C21orf54 IL10RB→ IFNGR2→ ←GART ←CRYZL1
LINC00945→ IFNAR2→ IFNAR1→ ←TMEM50B SON→ ITSN1→
OLIG1→ ←IL10RB−AS1 ←DNAJC28 ←DONSON
←LOC101928107 MIR6501→
Position on chr21 (Mb)

a


REACTOME_GPCR_LIGAND_BINDING
REACTOME_INTERFERON_SIGNALING
GO_RESPONSE_TO_VIRUS
REACTOME_G_ALPHA_I_SIGNALLING_EVENTS
GO_DEFENSE_RESPONSE_TO_VIRUS
GO_RESPONSE_TO_TUMOR_NECROSIS_FACTOR
HALLMARK_INTERFERON_GAMMA_RESPONSE
GO_RESPONSE_TO_INTERLEUKIN_1
GO_REGULATION_OF_VIRAL_LIFE_CYCLE
GO_RESPONSE_TO_INTERFERON_GAMMA
GO_EPITHELIAL_CELL_DEVELOPMENT
GO_REGULATION_OF_SYMBIOSIS_ENCOMPASSING_MUTUALISM_THROUGH_PARASITISM
REACTOME_ANTIVIRAL_MECHANISM_BY_IFN_STIMULATED_GENES
GO_REGULATION_OF_REPRODUCTIVE_PROCESS
GO_RESPONSE_TO_TYPE_I_INTERFERON
GO_REGULATION_OF_VIRAL_GENOME_REPLICATION
GO_VIRAL_GENOME_REPLICATION
GO_NEUROTRANSMITTER_BINDING
REACTOME_INTERFERON_ALPHA_BETA_SIGNALING
GO_NEGATIVE_REGULATION_OF_VIRAL_LIFE_CYCLE
HALLMARK_INTERFERON_ALPHA_RESPONSE
GO_NEGATIVE_REGULATION_OF_VIRAL_PROCESS
GO_NEUROPEPTIDE_SIGNALING_PATHWAY
GO_NEGATIVE_REGULATION_OF_VIRAL_GENOME_REPLICATION
GO_REGULATION_OF_NUCLEASE_ACTIVITY
GO_GLYCINE_BINDING
GO_NLS_BEARING_PROTEIN_IMPORT_INTO_NUCLEUS
GO_EPITHELIAL_CELL_PROLIFERATION_INVOLVED_IN_PROSTATE_GLAND_DEVELOPMENT
0.01
0.02
0.03
0.04
GeneRatio
Count
3
6
9
12
15
18
p.adjust
0.01
0.02
0.03
0.04

b

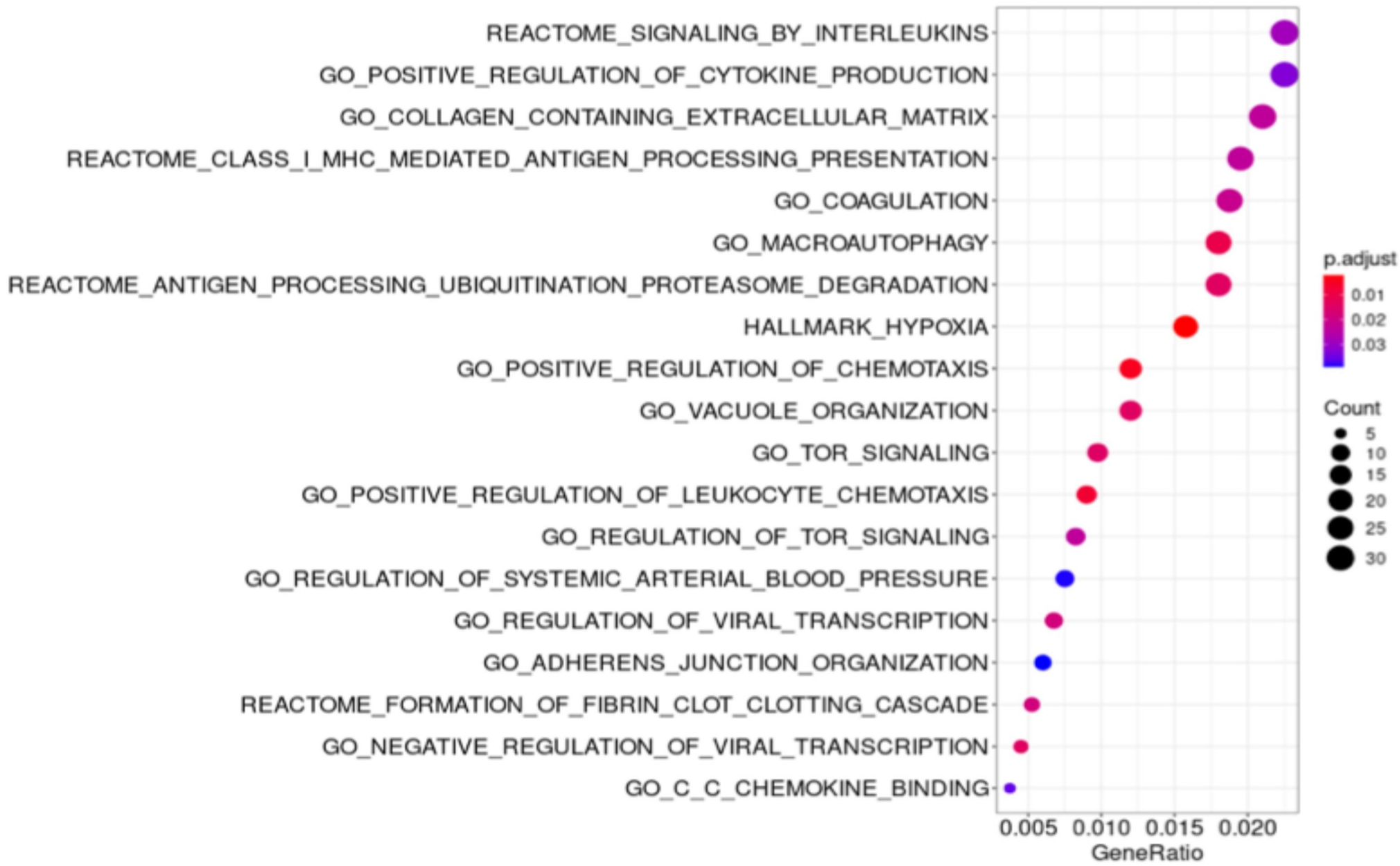
REACTOME_SIGNALING_BY_INTERLEUKINS
GO_POSITIVE_REGULATION_OF_CYTOKINE_PRODUCTION
GO_COLLAGEN_CONTAINING_EXTRACELLULAR_MATRIX
REACTOME_CLASS_I_MHC_MEDIATED_ANTIGEN_PROCESSING_PRESENTATION
GO_COAGULATION
GO_MACROAUTOPHAGY
REACTOME_ANTIGEN_PROCESSING_UBIQUITINATION_PROTEASOME_DEGRADATION
HALLMARK_HYPOXIA
GO_POSITIVE_REGULATION_OF_CHEMOTAXIS
GO_VACUOLE_ORGANIZATION
GO_TOR_SIGNALING
GO_POSITIVE_REGULATION_OF_LEUKOCYTE_CHEMOTAXIS
GO_REGULATION_OF_TOR_SIGNALING
GO_REGULATION_OF_SYSTEMIC_ARTERIAL_BLOOD_PRESSURE
GO_REGULATION_OF_VIRAL_TRANSCRIPTION
GO_ADHERENS_JUNCTION_ORGANIZATION
REACTOME_FORMATION_OF_FIBRIN_CLOT_CLOTTING_CASCADE
GO_NEGATIVE_REGULATION_OF_VIRAL_TRANSCRIPTION
GO_C_C_CHEMOKINE_BINDING
0.005
0.010
0.015
0.020
GeneRatio
p.adjust
0.01
0.02
0.03
Count
5
10
15
20
25
30

a

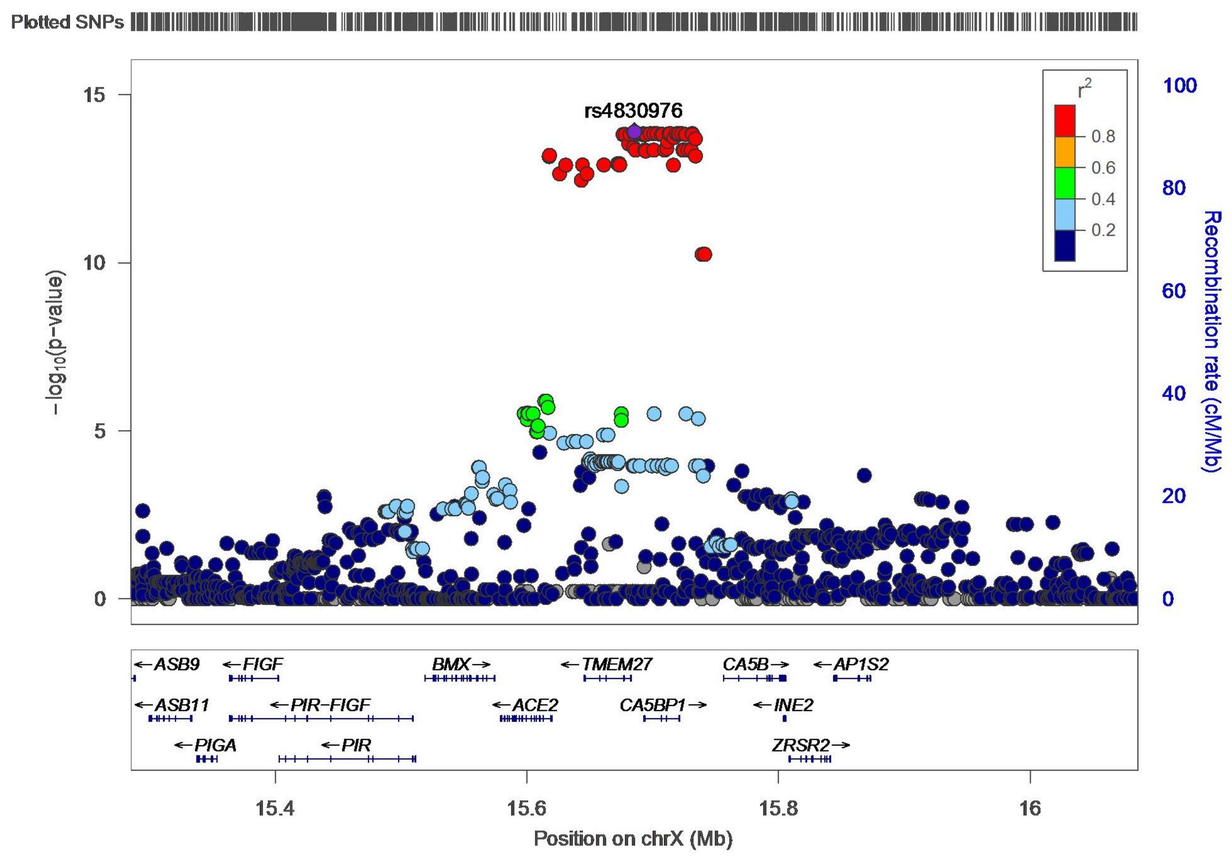
Plotted SNPs
rs4830976
r²
0.8
0.6
0.4
0.2
−log10(p−value)
Recombination rate (cM/Mb)
ASB9 FIGF BMX TMEM27 CA5B AP1S2
ASB11 PIR−FIGF ACE2 CA5BP1 INE2
PIGA PIR ZRSR2
Position on chrX (Mb)

b

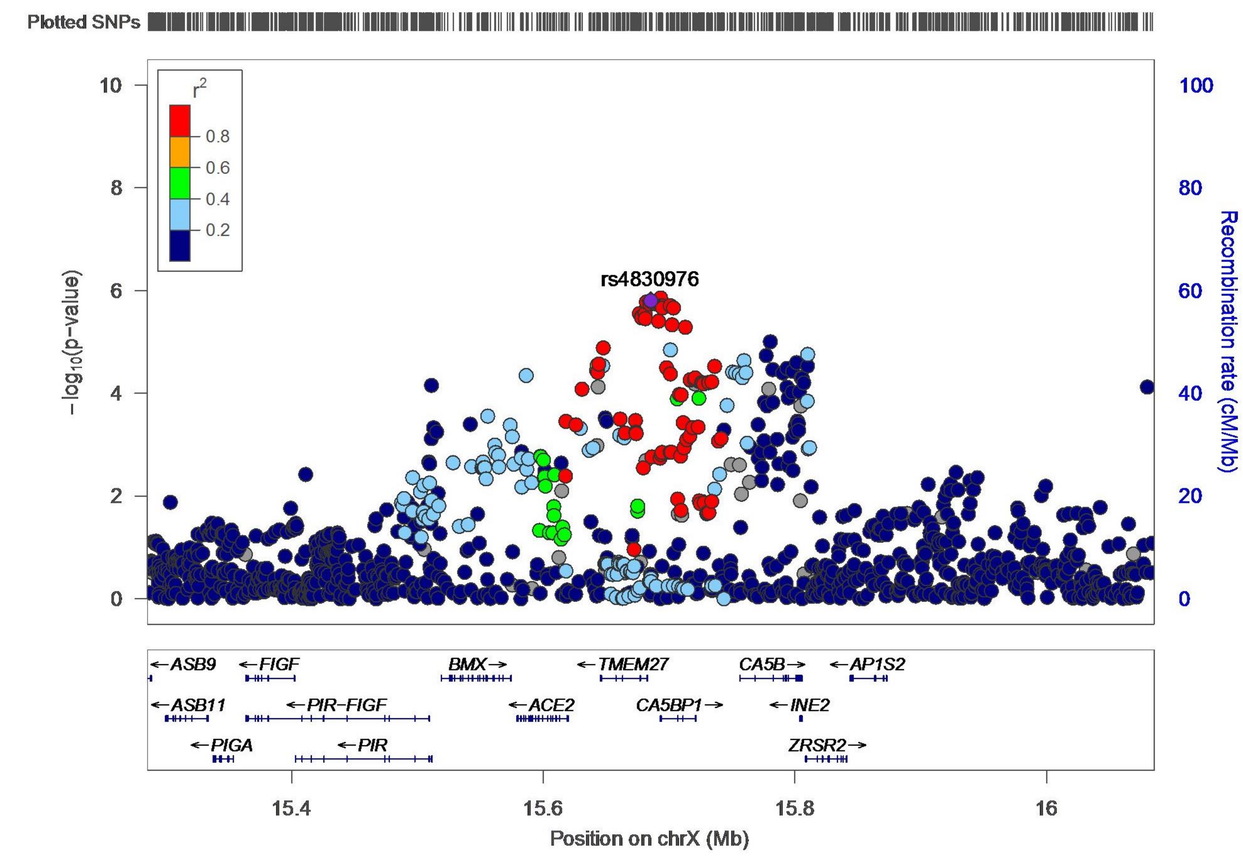
Plotted SNPs
rs4830976
r²
0.8
0.6
0.4
0.2
−log10(p−value)
Recombination rate (cM/Mb)
ASB9 FIGF BMX TMEM27 CA5B AP1S2
ASB11 PIR−FIGF ACE2 CA5BP1 INE2
PIGA PIR ZRSR2
Position on chrX (Mb)

c

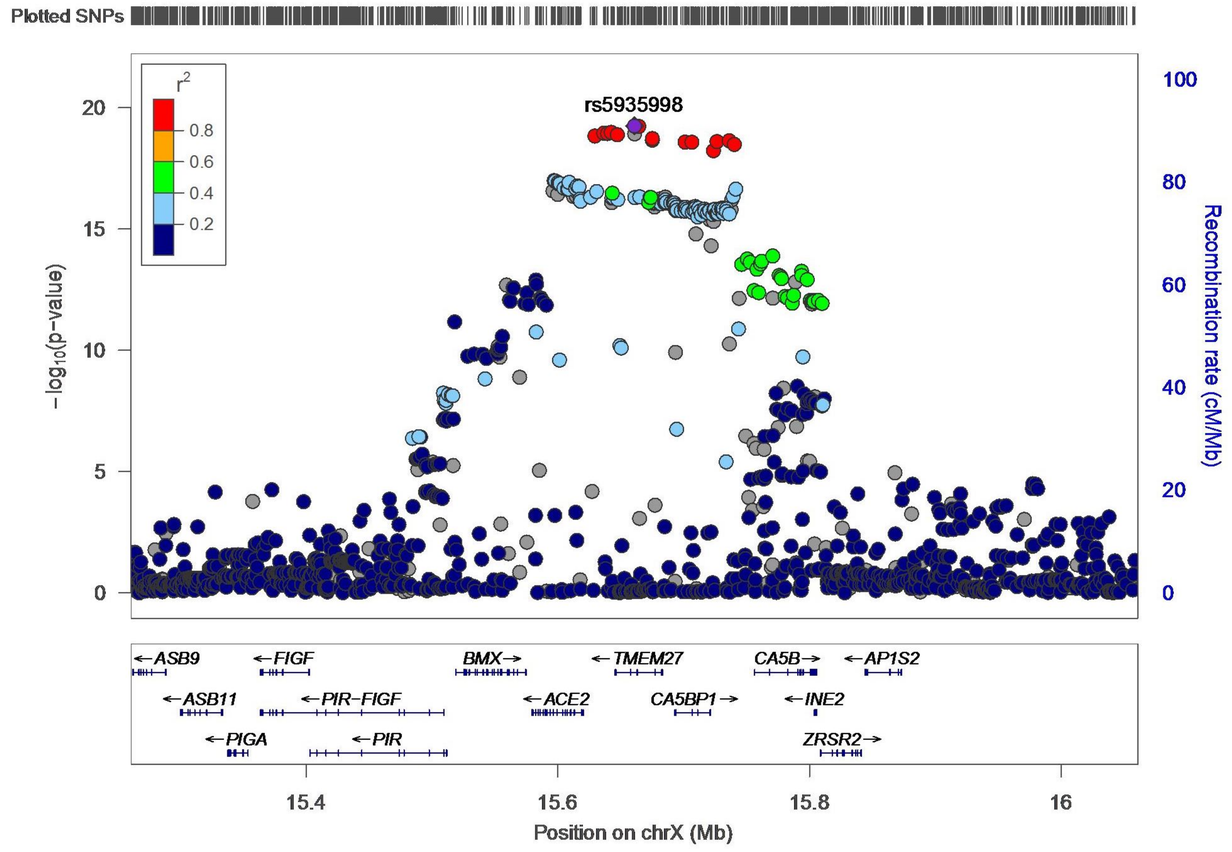
Plotted SNPs
rs5935998
r²
0.8
0.6
0.4
0.2
−log10(p−value)
Recombination rate (cM/Mb)
ASB9 FIGF BMX TMEM27 CA5B AP1S2
ASB11 PIR−FIGF ACE2 CA5BP1 INE2
PIGA PIR ZRSR2
Position on chrX (Mb)

d

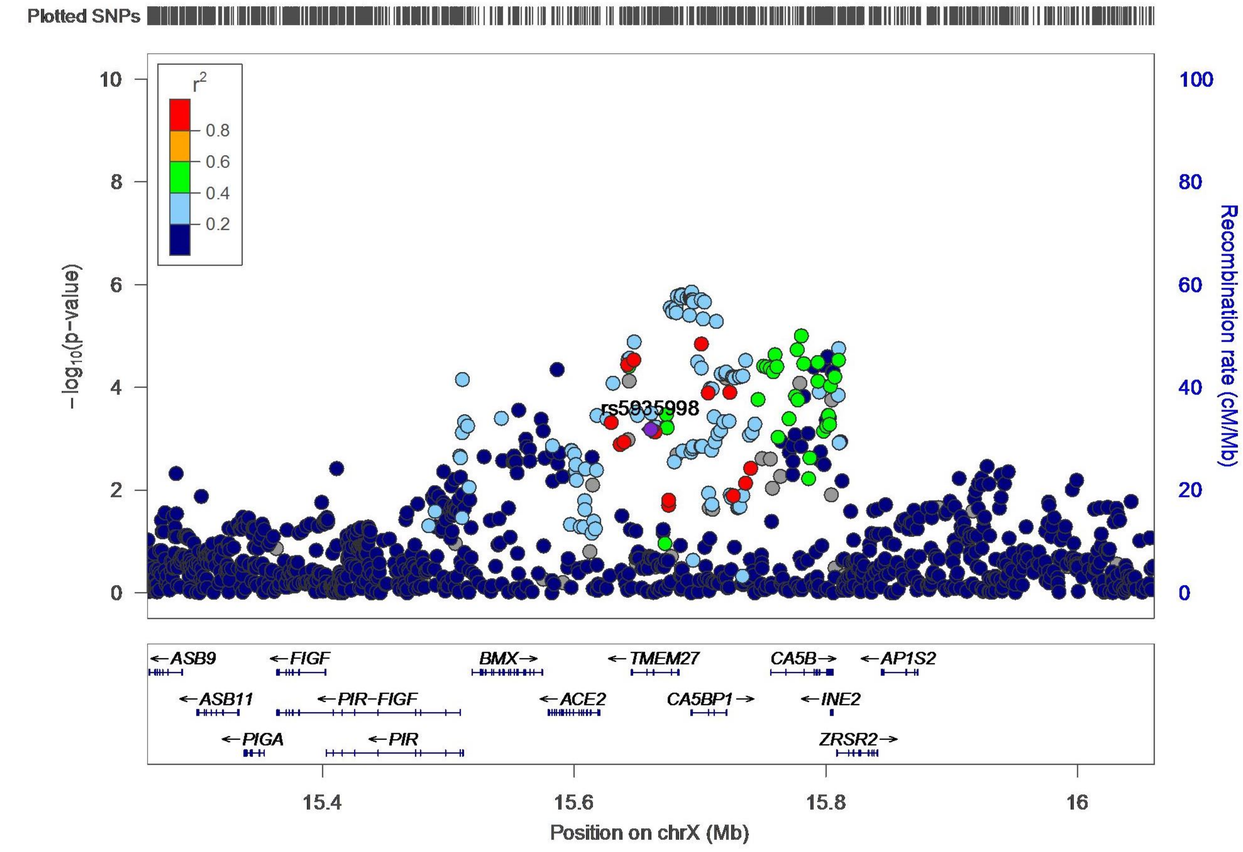
Plotted SNPs
rs5935998
r²
0.8
0.6
0.4
0.2
−log10(p−value)
Recombination rate (cM/Mb)
ASB9 FIGF BMX TMEM27 CA5B AP1S2
ASB11 PIR−FIGF ACE2 CA5BP1 INE2
PIGA PIR ZRSR2
Position on chrX (Mb)

e

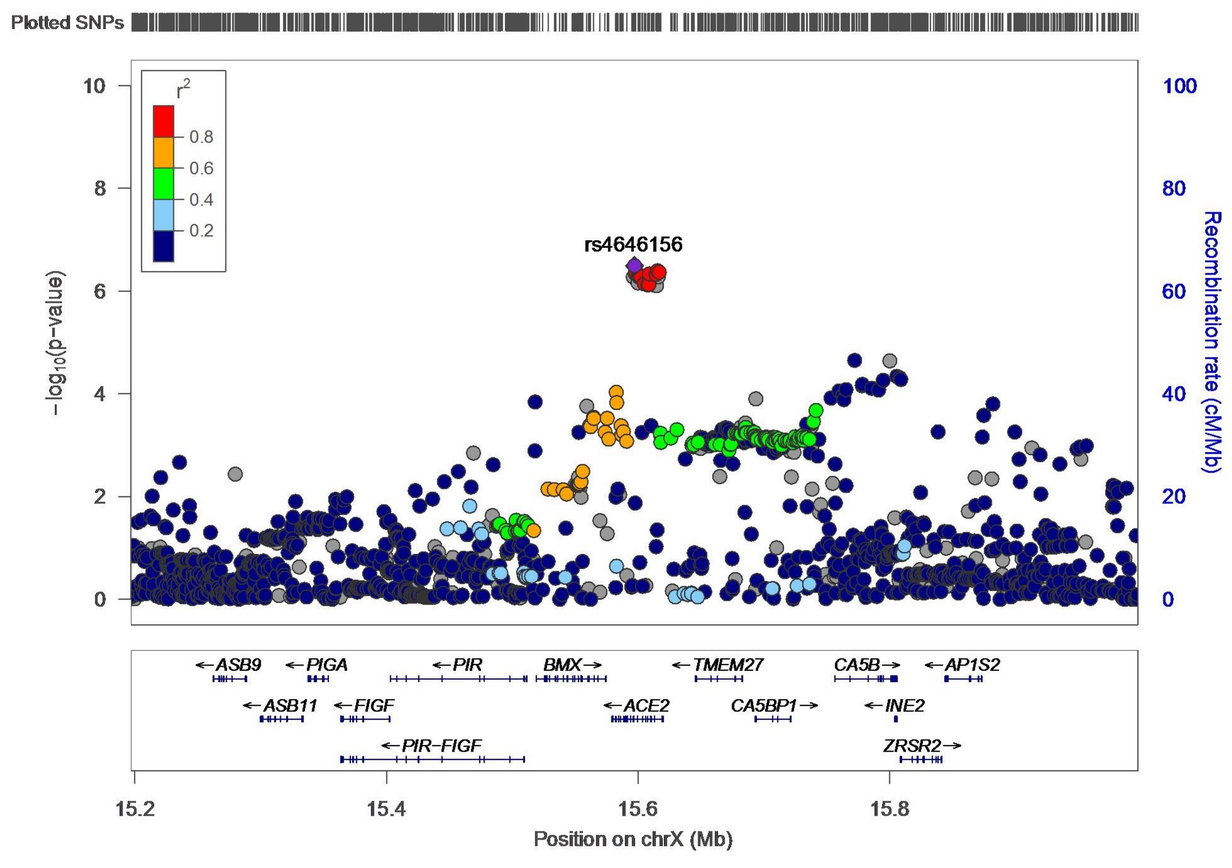
Plotted SNPs
rs4646156
r²
0.8
0.6
0.4
0.2
−log10(p−value)
Recombination rate (cM/Mb)
ASB9 PIGA PIR BMX TMEM27 CA5B AP1S2
ASB11 FIGF ACE2 CA5BP1 INE2
PIR−FIGF ZRSR2
Position on chrX (Mb)

f

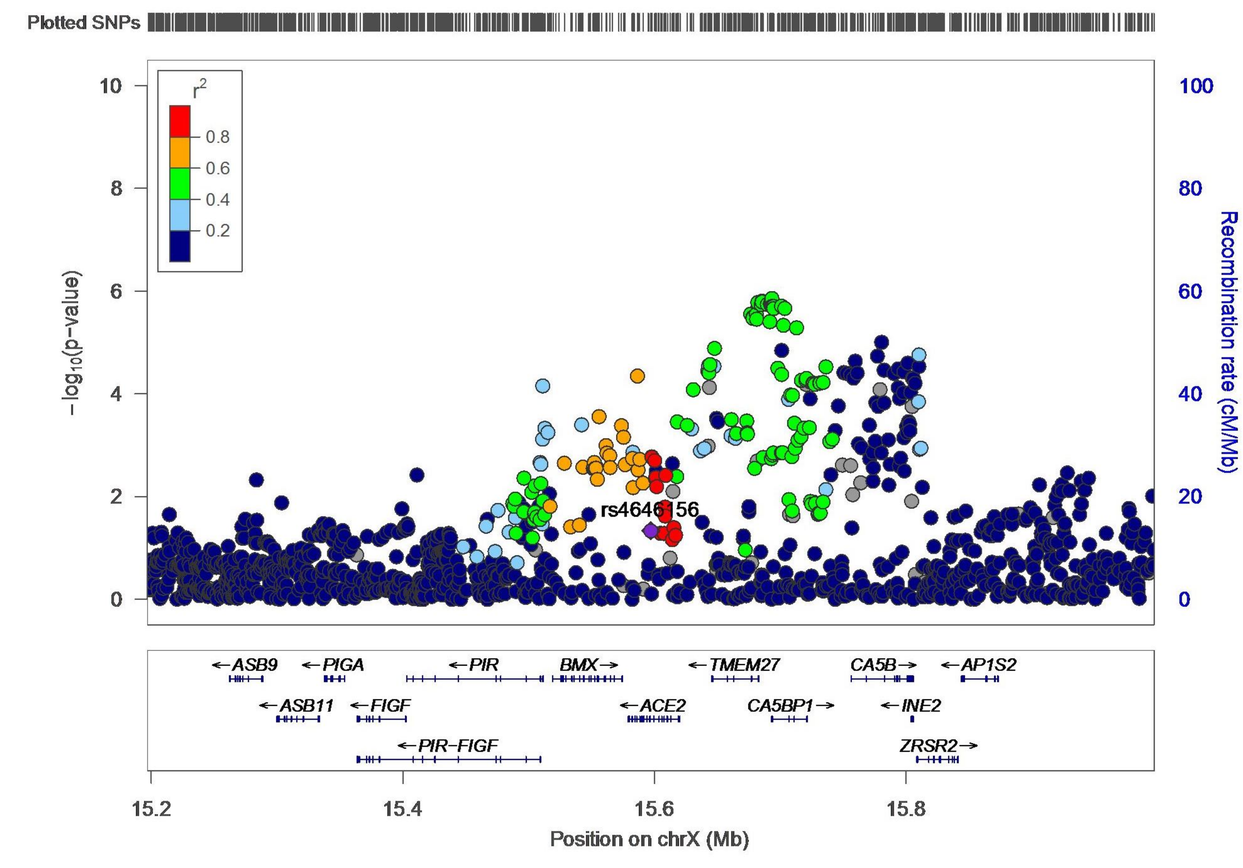
Plotted SNPs
rs4646156
r²
0.8
0.6
0.4
0.2
−log10(p−value)
Recombination rate (cM/Mb)
ASB9 PIGA PIR BMX TMEM27 CA5B AP1S2
ASB11 FIGF ACE2 CA5BP1 INE2
PIR−FIGF ZRSR2
Position on chrX (Mb)